Experimental Study of Plasma Transport Using X-ray Imaging Crystal Spectrometer in Alcator C-Mod

Chi Gao

Thesis Supervisor: Dr. John E. Rice

In collaboration with M.L. Reinke, L Delgado-Aparicio, Y.A. Podpaly, H.J. Sun and Alcator C-Mod team.

April 13, 2015

Overview

1. X-ray Imaging Crystal Spectroscopy System in Alcator C-Mod
2. Impurity (Argon) Control and Pumpout
3. Rotation Reversal and Non-local Heat Transport
4. Future Work on Spectroscopy

Overview

X-ray Imaging Spectroscopy System in Alcator C-Mod

HiReX–SR: **Hi**gh **Re**solution **X**-ray Spectrometer with **S**patial **R**esolution

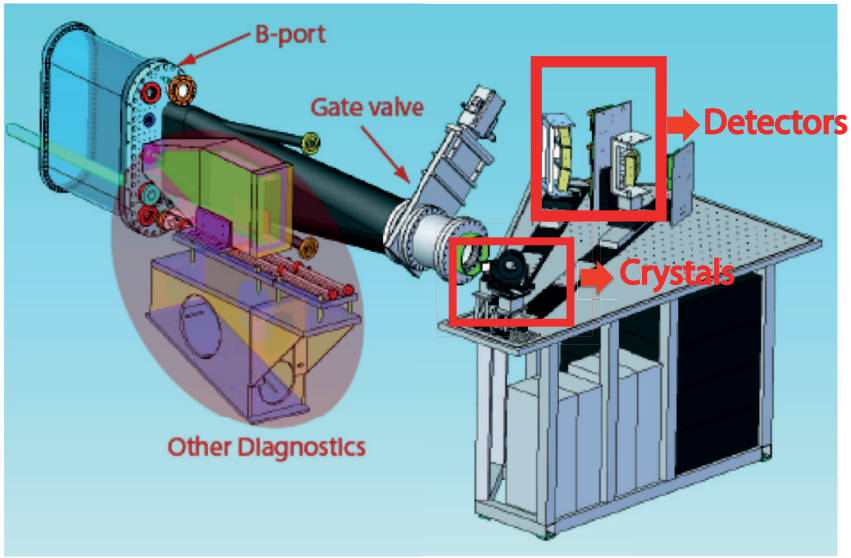

Hardware:
Pioneered by Bitter, Hill (1999).
Built by Ince-Cushman, Rice and Podpaly.

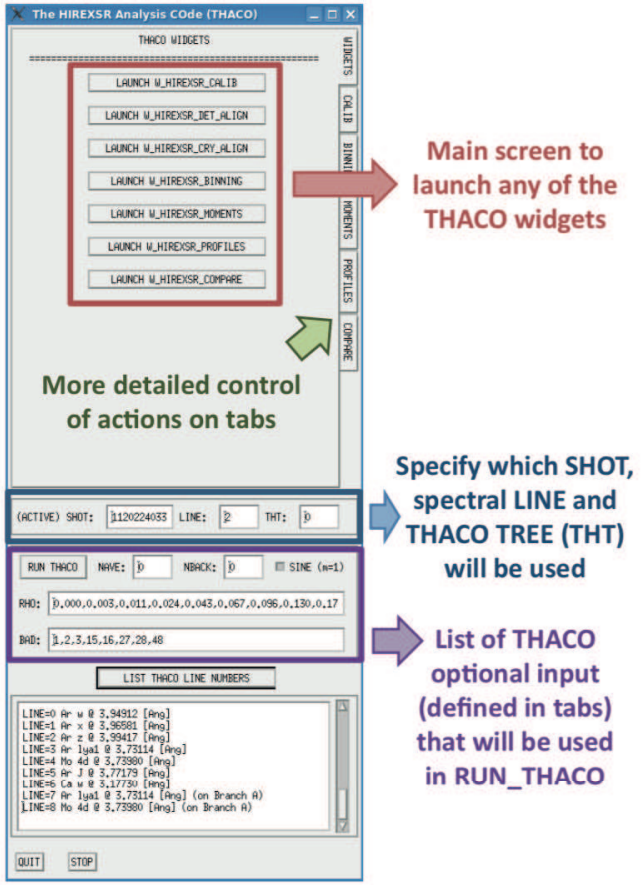

Software:
THACO (Reinke, Podpaly, Gao).

HiReX–SR

- Motivations:
  - Interested in $T_i(r), V_i(r), E_r(r)$.
  - CXRS with neutral beam may not be feasible for high density plasma.
  - X-ray spectrometer with spatial resolution can provide $T_I(r), V_I(r), T_e(r), \epsilon_I(r), E_r(r)$ information.

- Spherically bent crystal:
  - Increase the photon throughput (v.s. flat crystal).
  - Provide spatial resolution (v.s. cylindrical crystal).

- Argon: Ar^{16+} and Ar^{17+} are dominant charge states at $T_e = 0.5$ - 6 keV.

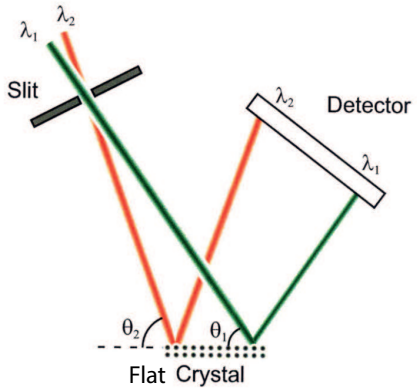

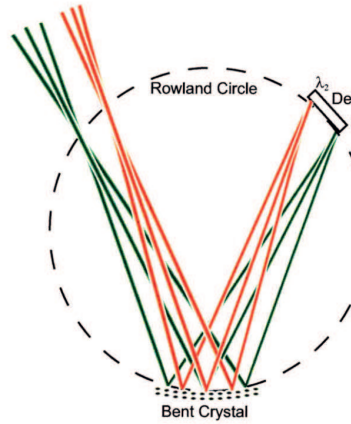

M. Bitter *et al. Review of scientific instruments* **70**, 292 (1999)
A. Ince-Cushman *et al. Review of scientific instruments* **79**, 10E302 (2008)

HiReX–SR

- Motivations:
  - Interested in $T_i(r), \mathbf{V}_i(r), E_r(r)$.
  - CXRS with neutral beam may not be feasible for high density plasma.
  - X-ray spectrometer with spatial resolution can provide $T_I(r), \mathbf{V}_I(r), \epsilon_I(r), T_e(r), E_r(r)$ information.

- Spherically bent crystal:
  - Increase the photon throughput (v.s. flat crystal).
  - Provide spatial resolution (v.s. cylindrical crystal).

- Argon: Ar^{16+} and Ar^{17+} are dominant charge states at $T_e = 0.5$ - 6 keV.

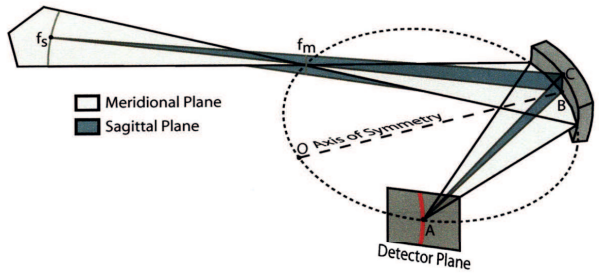

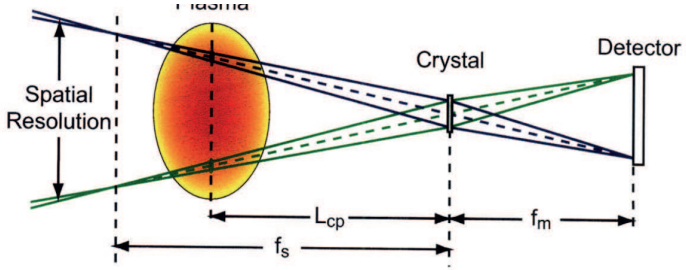

HiReX–SR

- Motivations:
  - Interested in $T_i(r), V_i(r), E_r(r)$.
  - CXRS with neutral beam may not be feasible for high density plasma.
  - X-ray spectrometer with spatial resolution can provide $T_I(r), V_I(r), \epsilon_I(r), T_e(r), E_r(r)$ information.
- Spherically bent crystal:
  - Increase the photon throughput (v.s. flat crystal).
  - Provide spatial resolution (v.s. cylindrical crystal).
- Argon: Ar^{16+} and Ar^{17+} are dominant charge states at $T_e = 0.5$ - 6 keV.

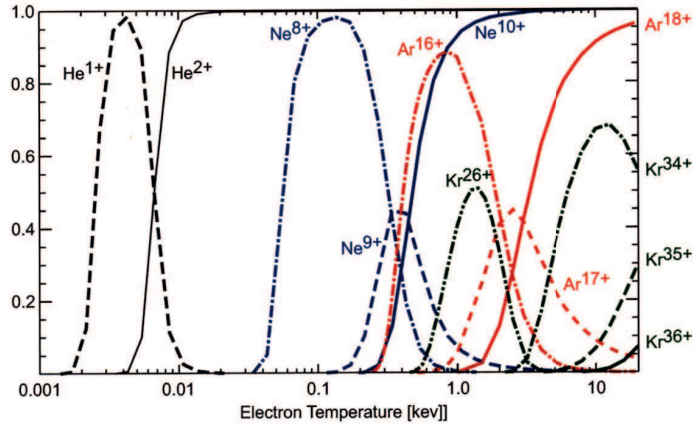

THACO: **T**he **H**iReX-SR **A**nalysis **CO**de

THACO: analyze the HiReX–SR data to get $\epsilon(r,t)$, $V_\Phi(r,t)$ and $T_I(r,t)$.

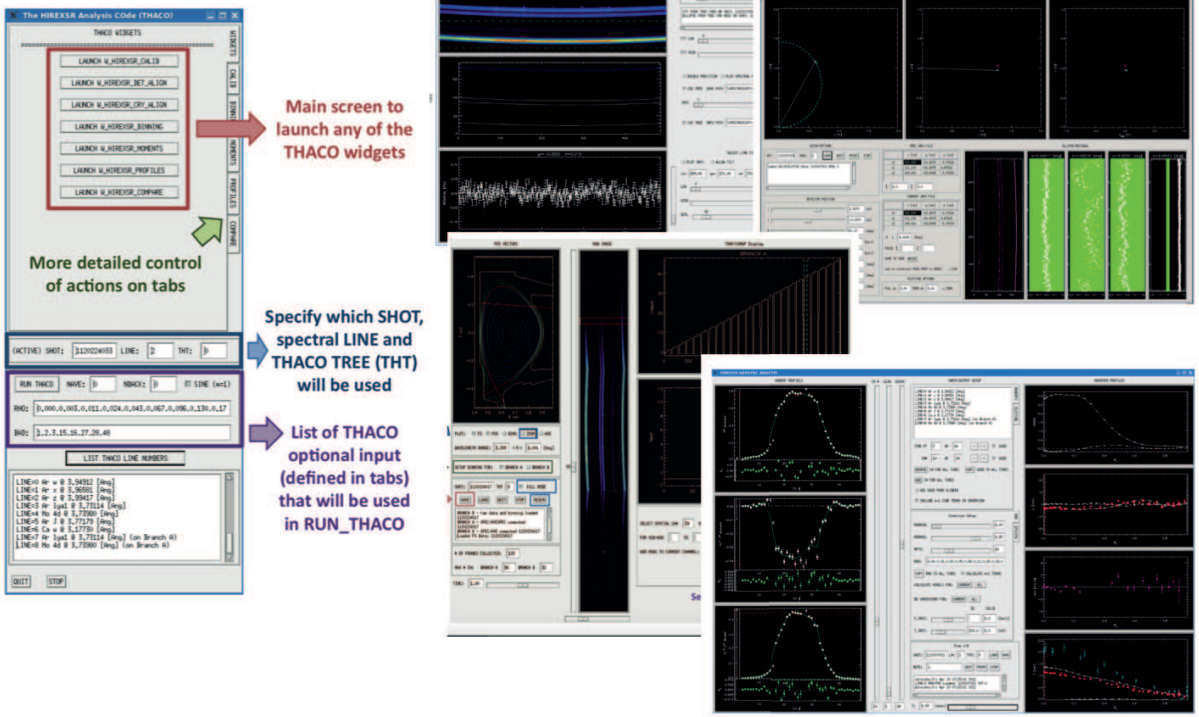

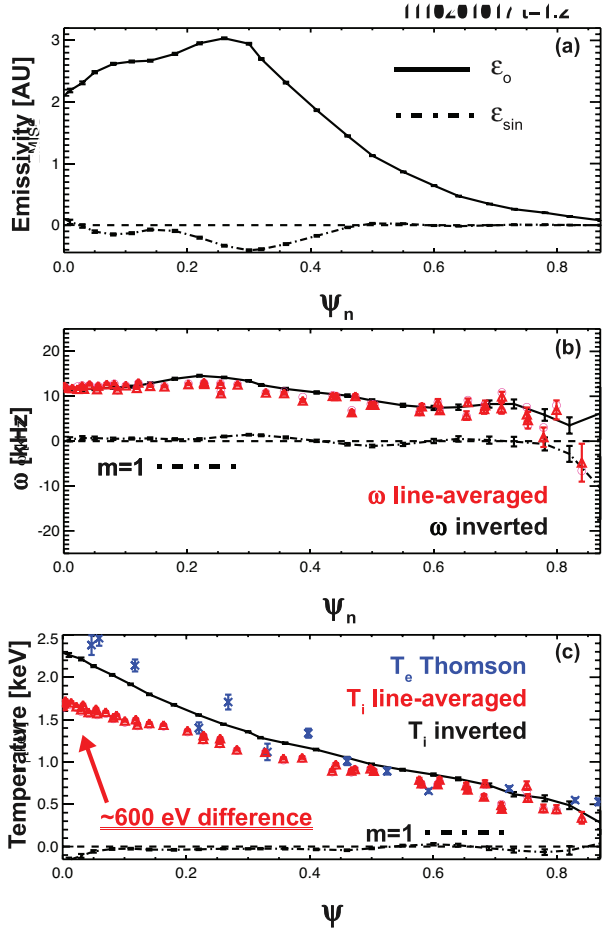

M.L. Reinke *et al. Review of Scientific Instruments* **83**, 113504 (2012)

Overview

Key Results

- Argon level is strongly reduced with ICRF in H–D plasmas.
- Argon pumpout effect is maximal at $n_H/n_D \approx 42 \pm 5\%$.
- Argon pumpout effect has a 0.5 MW ICRF power threshold.
- Impurity-wave interaction and edge effects are possible mechanisms.

Paper to be submitted.

Motivation: Radiation & Impurity Control

- Impurity types:

Type	**Example**
Intrinsic (non-recycling)	B, Mo
Non-intrinsic (non-recycling)	Ca
Non-intrinsic (recycling)	Ne, Ar

- Impurities dilute plasmas. Energy loss by impurity radiation could affect the plasma performance, and even cause disruptions.
- A phenomenon potentially useful for active recycling impurity control is observed.

Argon Intensity Strongly Decreases during ICRF

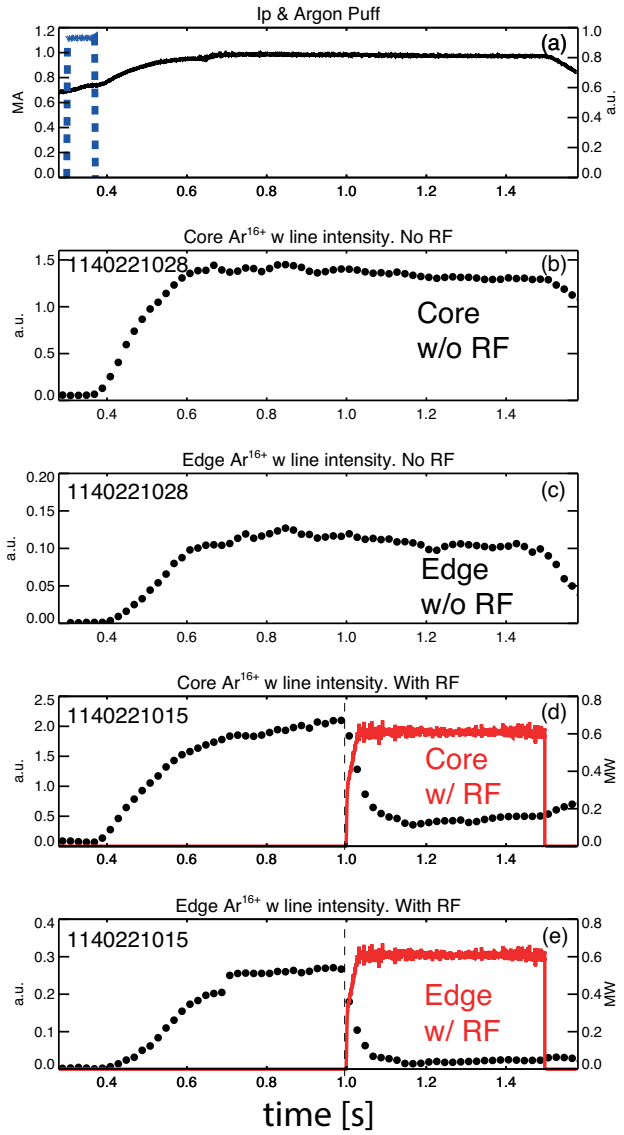

- (a) Argon puff at 0.3 s for 75 ms (blue line).
- (b, c) Without ICRF, core and edge argon intensity is steady (due to recycling).
- (d, e) With ICRF (red line, 0.6 MW ICRF), core and edge argon intensities strongly decrease (with decay time $\sim$ 50 ms).

There is a Preferred n_H/n_D for the Pumpout Effect

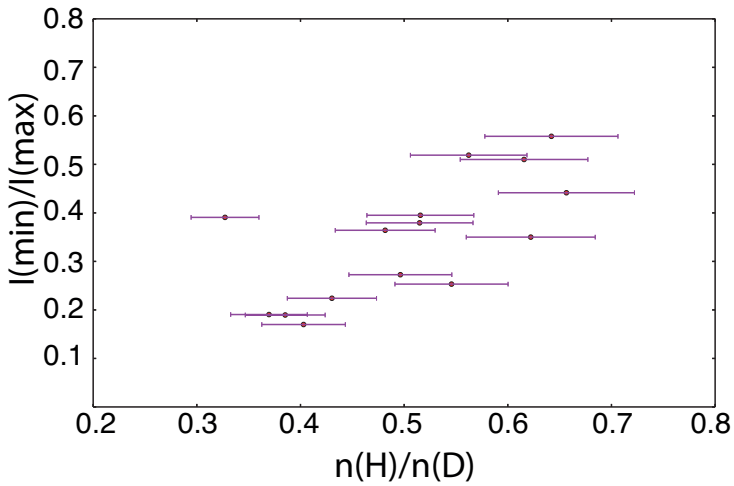

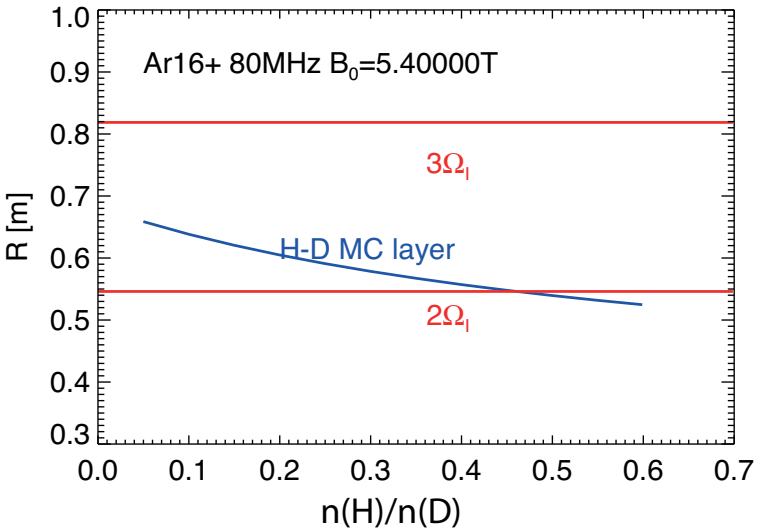

- Pumpout only in plasmas with relatively high H/D ratio.
- An optimum $\frac{n_H}{n_D} \approx 42 \pm 5\%$.
- $\frac{n_H}{n_D} = 46\%$ H-D mode conversion layer overlaps with Ar^{16+} 2^{nd} harmonic resonance layer.

There is a Preferred n_H/n_D for the Pumpout Effect

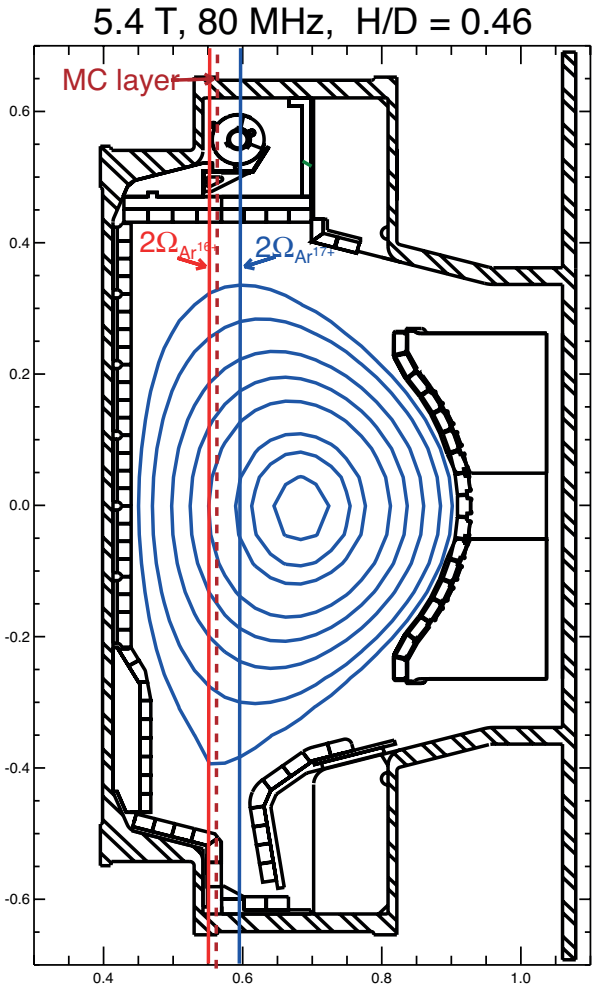

- Pumpout only in plasmas with relatively high H/D ratio.
- An optimum $\frac{n_H}{n_D} \approx 42 \pm 5\%$.
- $\frac{n_H}{n_D} = 46\%$ H-D mode conversion layer overlaps with Ar^{16+} 2^{nd} harmonic resonance layer.

A Power Threshold for Pumpout Effect

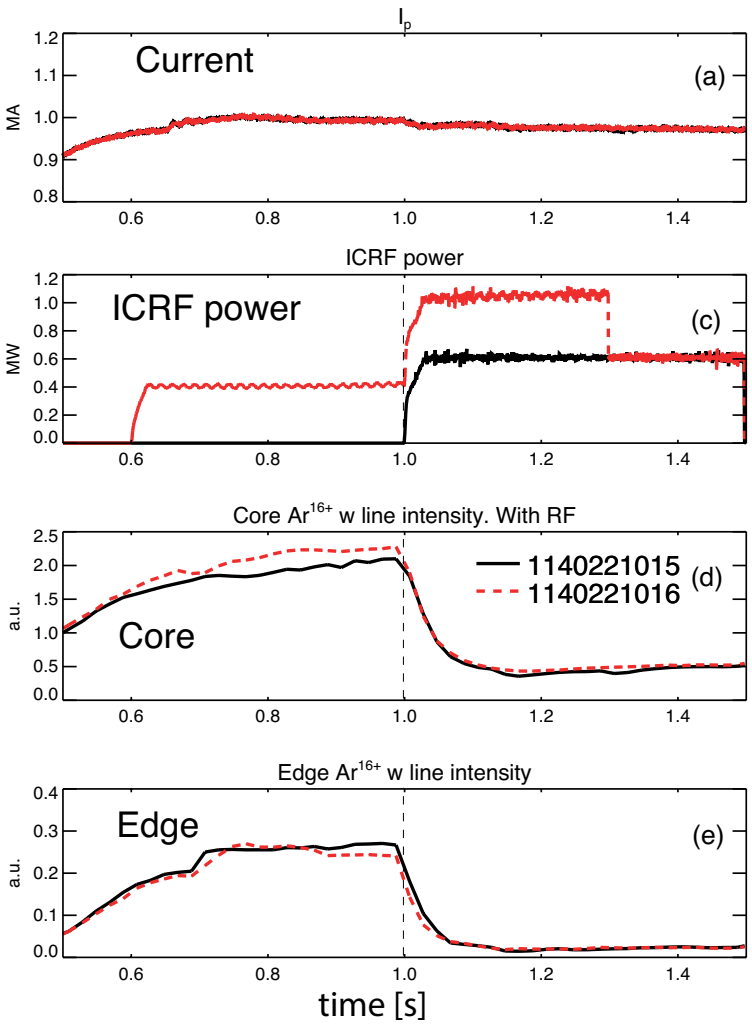

- No pumpout when $P_{ICRF} < 0.5$ MW
- Pumpout when $P_{ICRF} > 0.5$ MW

Argon Intensity Recovers when ICRF Turns Off

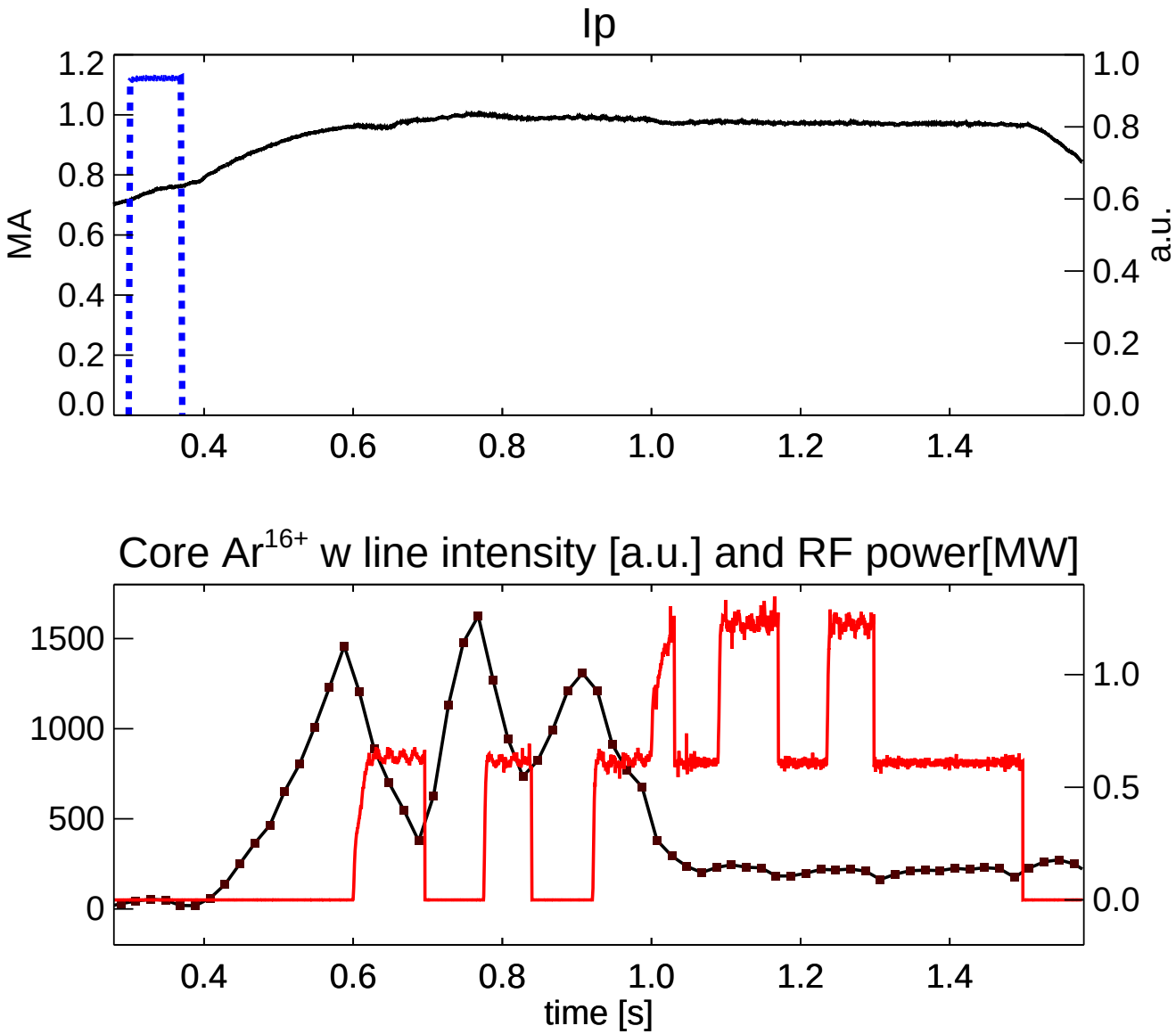

Mo Injection and Non-Resonant Lines

Molybdenum intensity increases.

Emission lines from non-resonant argon charge states also decrease with strength similar to resonant argon lines.

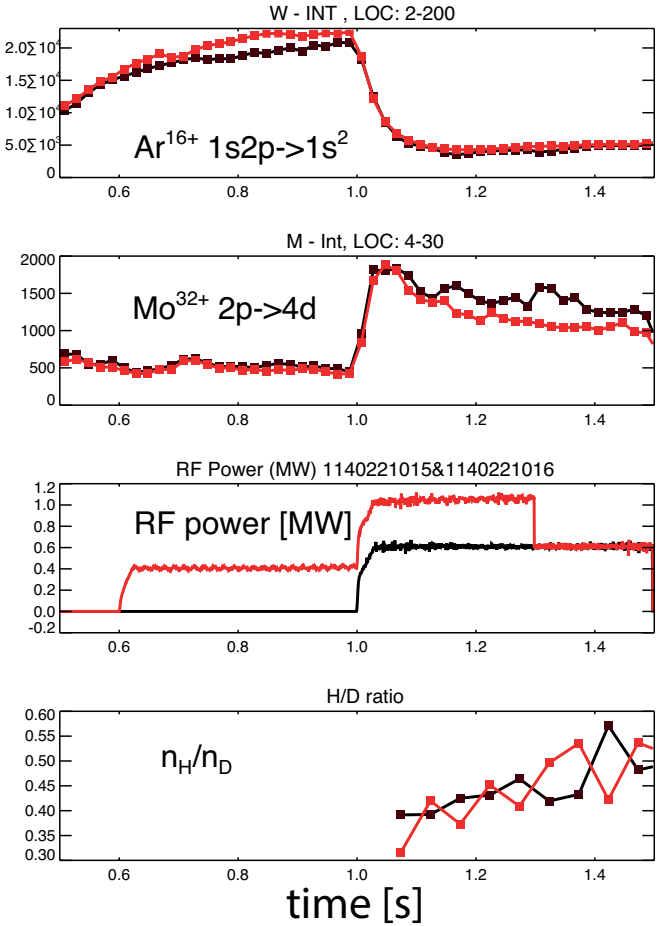

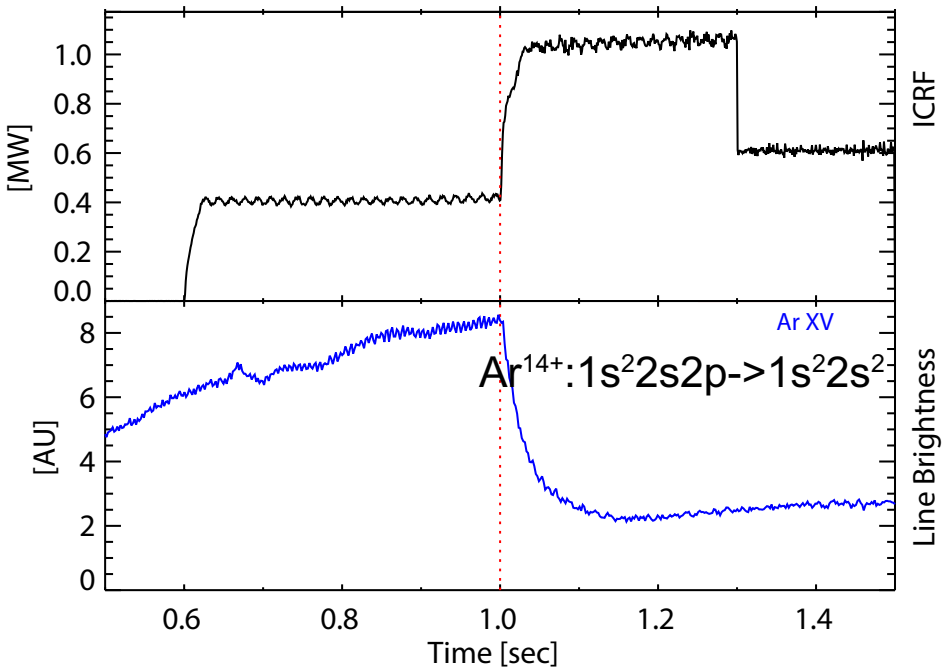

Profiles don't Change Significantly

- T_e increases, then drops $\sim 10\%$.
- T_I increases $\sim 10\%$.
- n_e unchanged.
- Changes in neoclassical and turbulent particle transport should be small.

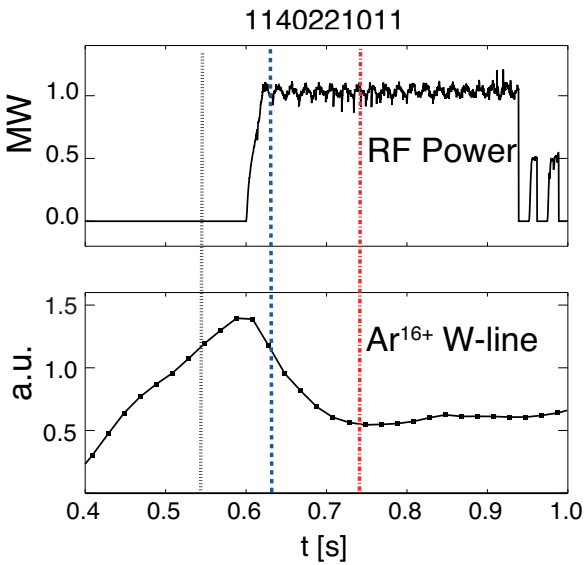

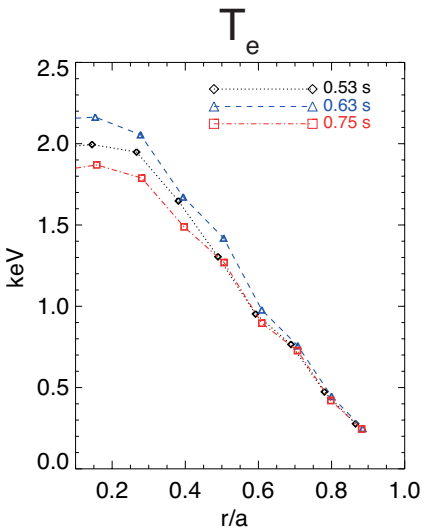

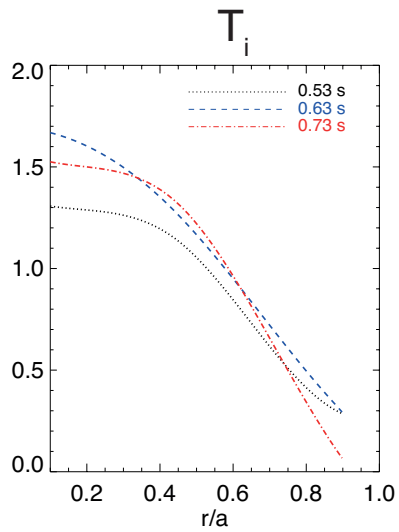

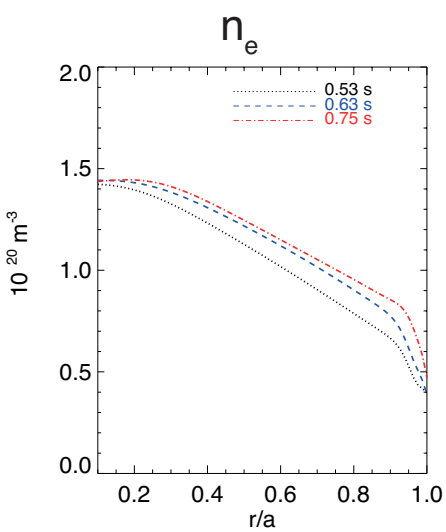

Possible Mechanisms

1. Impurity-RF wave interaction.
   - A preferred $n_H/n_D \approx 42 \pm 5\%$.
   - A power threshold.
   - Argon intensity is modulated by ICRF.
2. Edge effect: changes in edge source/recycling.
   - Plasma edge potential may change the impurity influx.
   - Wall recycling could be modified by ICRF.
3. Transport effect: changes in T_e, T_i or n_e.
   - n_e unchanged.
   - T_e increases then drops $\sim 10\%$.
   - T_i increases $\sim 10\%$.
   - Gradient changes are small.

STRAHL Simulation

STRAHL is used to test the edge source effect.

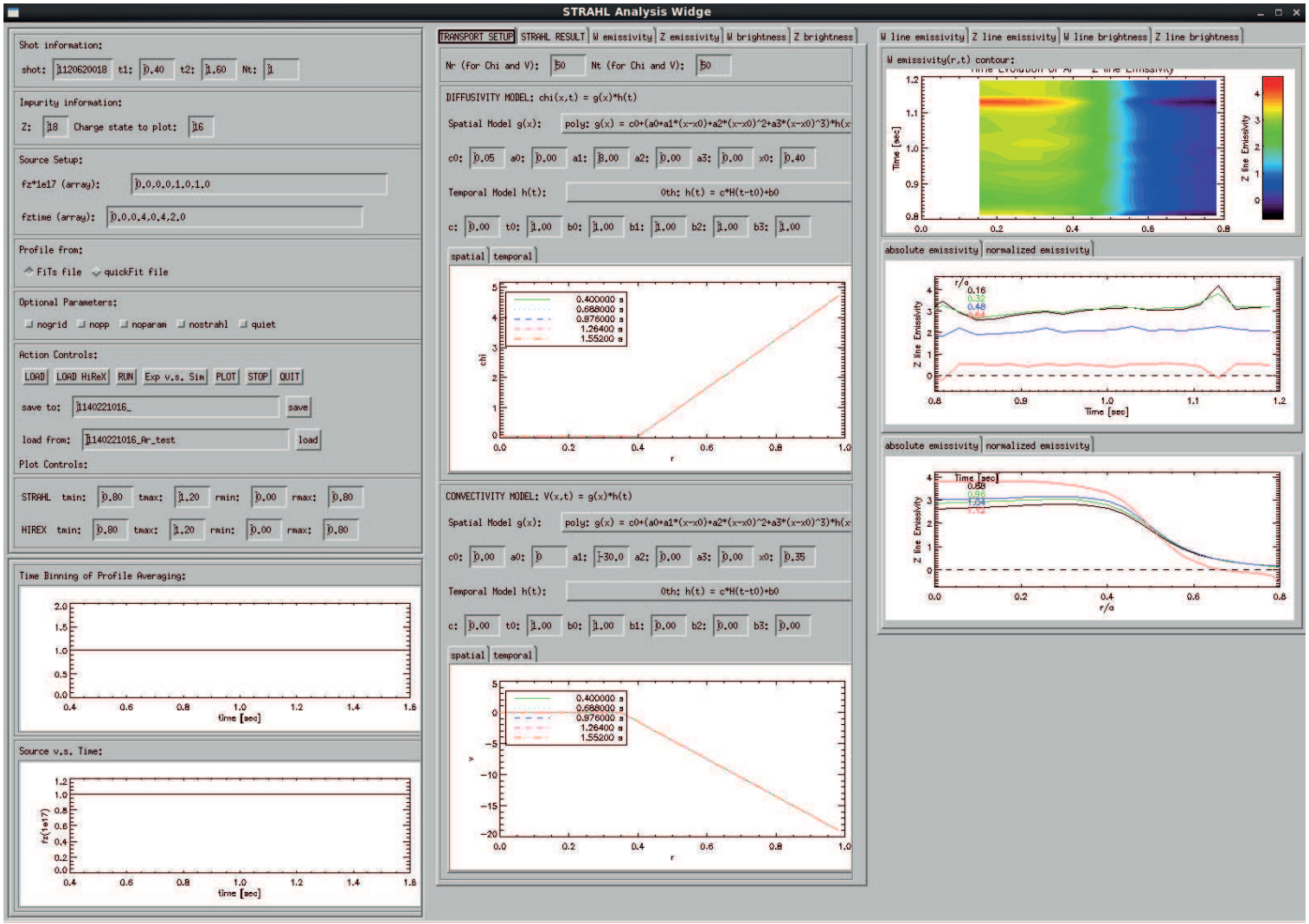

Simulation with Source Reduction

Simulation with a reduction in source qualitatively reproduces the evolution of argon brightness.

STRAHL(normalized)

D=1 m/s^2, Source$_{t\geq 1.0}$ $\sim$ 0.3$\times$ Source$_{t<1.0}$

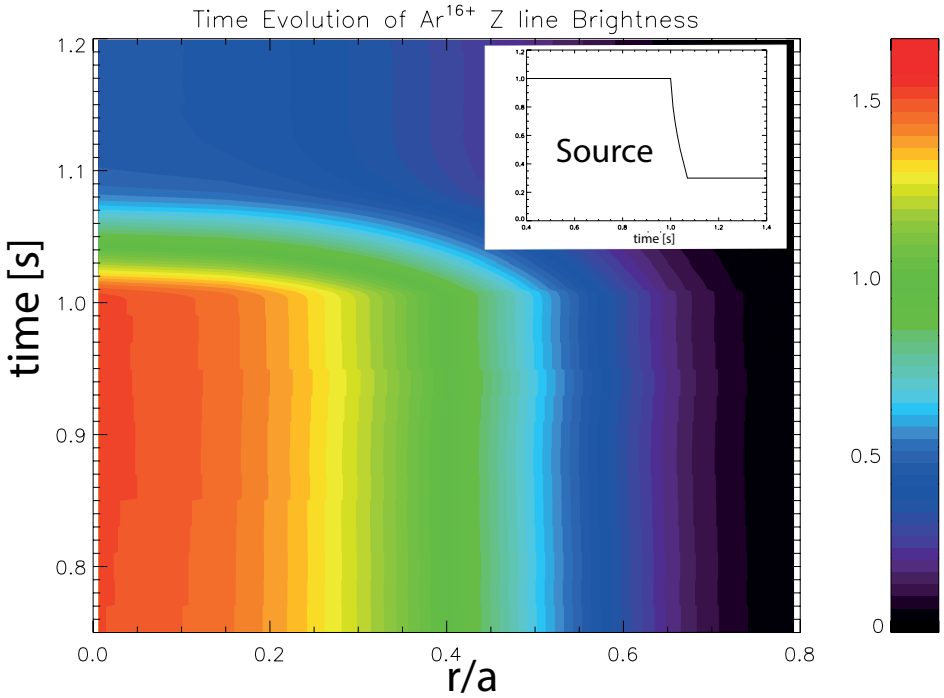

Experiment (HiReX–SR)

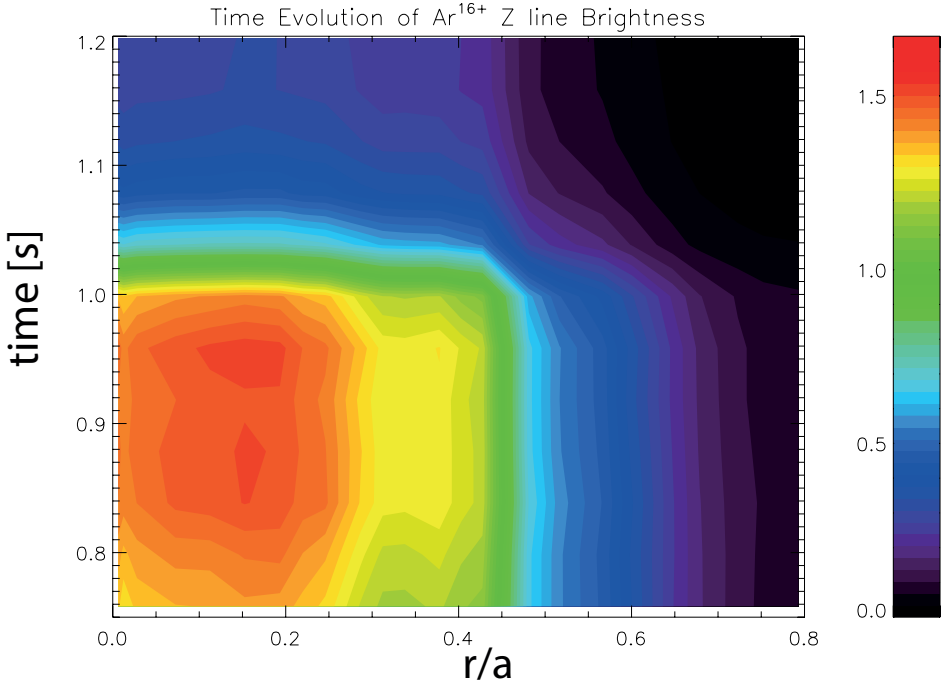

Simulation with Source Reduction

The evolutions of normalized brightness show agreement between STRAHL simulation and experiment.

STRAHL(normalized)

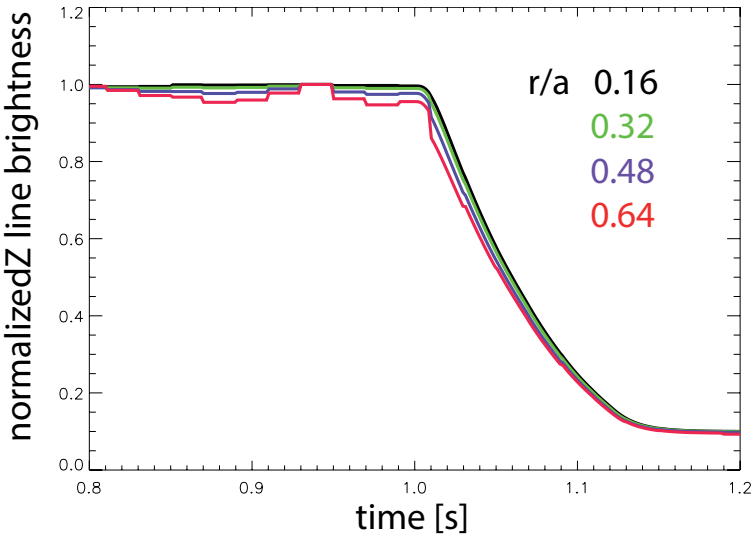

Experiment (HiReX–SR)

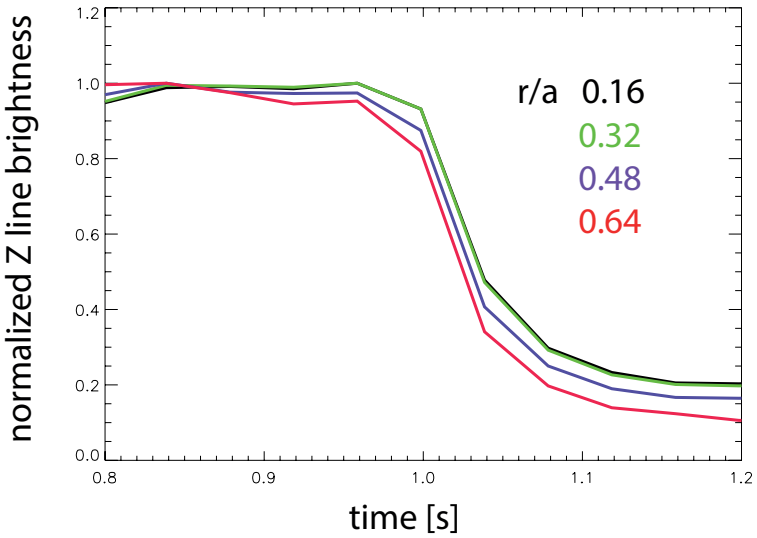

Summary of Argon Pumpout

- Argon level is strongly reduced with ICRF in H–D plasmas.
  1. A preferred $n_H/n_D \approx 42 \pm 5\%$.
  2. A power threshold.
  3. Argon intensity is modulated by ICRF.
  4. Coupled with molybdenum injection.
- Impurity-wave interaction and source/edge effect are the most probable reasons.
  1. Impurity-wave interaction: Probable
  2. Source/edge effect: Maybe
  3. Change of other plasma parameter: Not relevant
- Future work (May 2015)
  1. Experiment with PCI is planned to identify the mode conversion strength and location.
  2. Edge diagnostics (chromex, scanning probe, etc.) will be employed to monitor edge effects.

Overview

Key Results

- Non-local heat transport is observed in Alcator C-Mod with a density threshold.
- The non-local effect is correlated with **rotation reversal** and **LOC-SOC transition**.

C. Gao *et al. Nuclear Fusion* **54**, 083025 (2014)
J.E. Rice *et al. Nuclear Fusion* **53**, 033004 (2013)

Rotation Reversal and LOC/SOC Transition

- Rotation reversal is intensively studied in Alcator C-Mod.
- LOC/SOC transition and rotation reversal are correlated.
- A hypothesis: TEM to ITG.
- Recent cold pulse experiments extend the connection to include non-local heat transport.

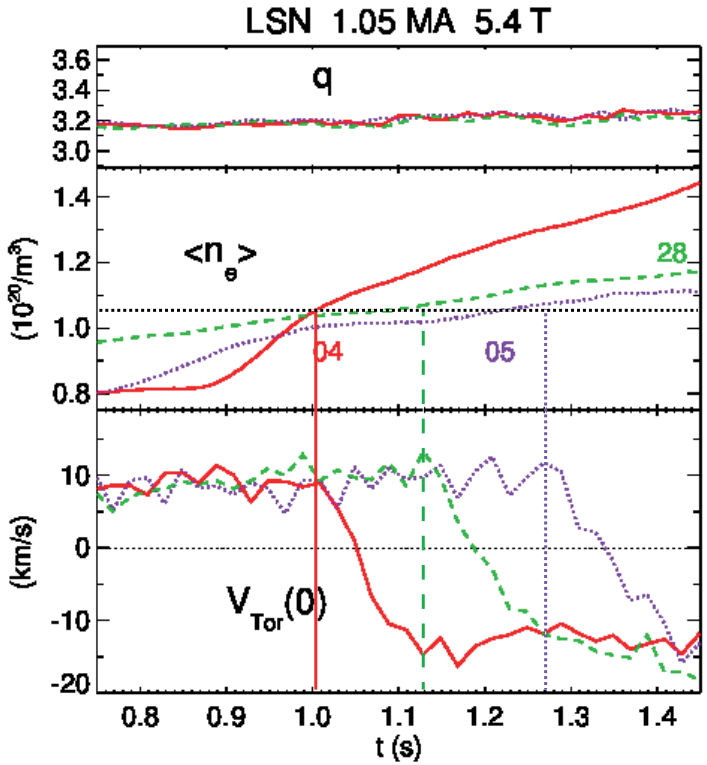

J.E. Rice *et al.* *Physical Review Letters* **107**, 265001 (2011)
J.E. Rice *et al.* *Nuclear Fusion* **51**, 083005 (2011)
J.E. Rice *et al.* *Physics of Plasmas* **19**, 056106 (2012)

Rotation Reversal and LOC/SOC Transition

- Rotation reversal is intensively studied in Alcator C-Mod.
- LOC/SOC transition and rotation reversal are correlated.
- A hypothesis: TEM to ITG.
- Recent cold pulse experiments extend the connection to include non-local heat transport.

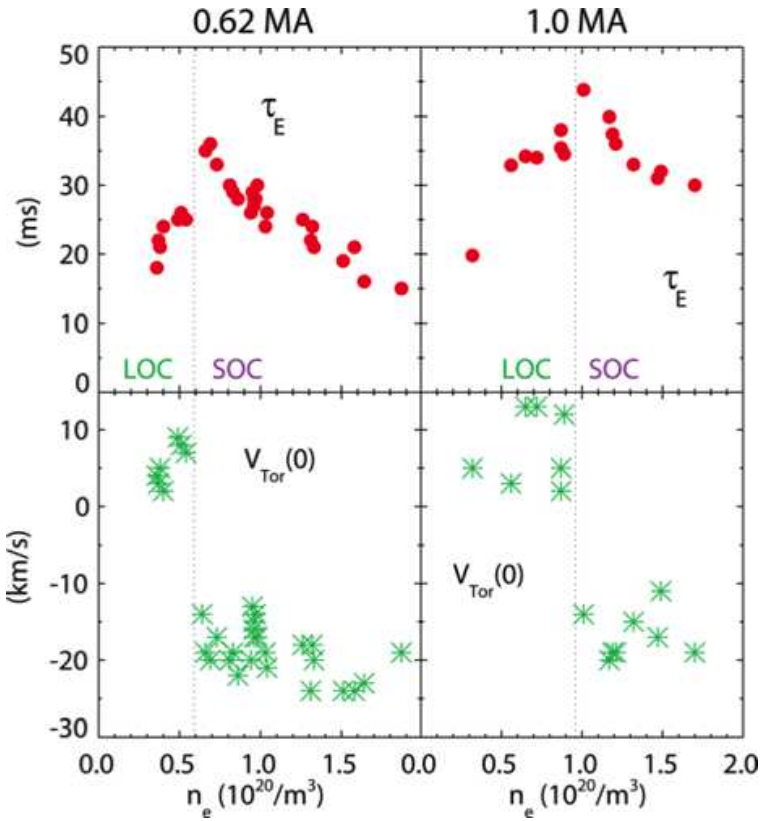

Rotation Reversal and LOC/SOC Transition

- Rotation reversal is intensively studied in Alcator C-Mod.
- LOC/SOC transition and rotation reversal are correlated.
- A hypothesis: TEM to ITG.
- Recent cold pulse experiments extend the connection to include non-local heat transport.

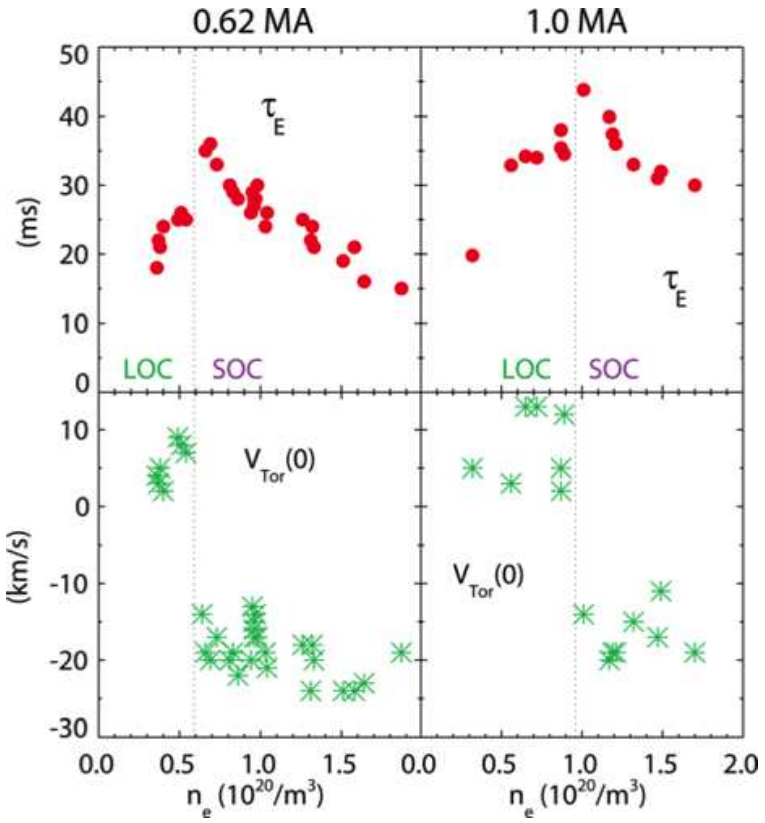

Cold Pulse in LOC and SOC Plasmas

- In low density LOC plasmas, core T_e **peaks** in $\sim$ 10 ms, much shorter than energy confinement time $\sim$ 23 ms.
- In high density SOC plasmas, the cold response evolution time ($\sim$ 30 ms) is comparable with energy confinement time $\sim$ 27ms.

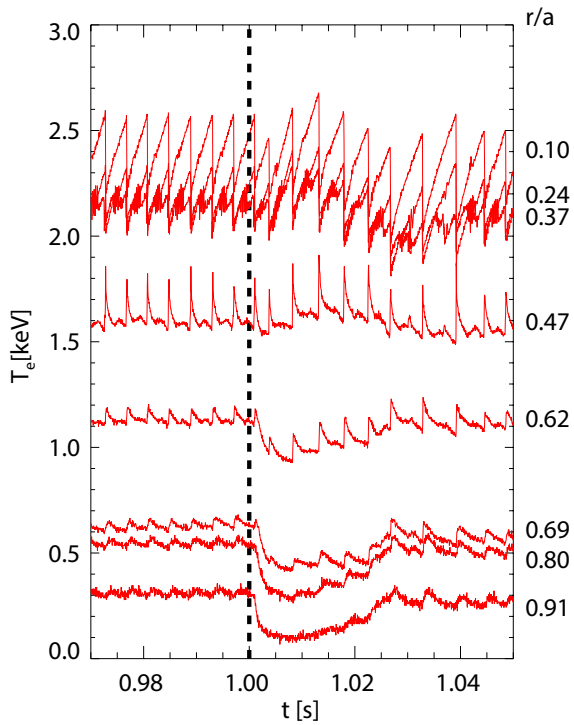

LOC: $\bar{n}_{e,20} = 0.6$

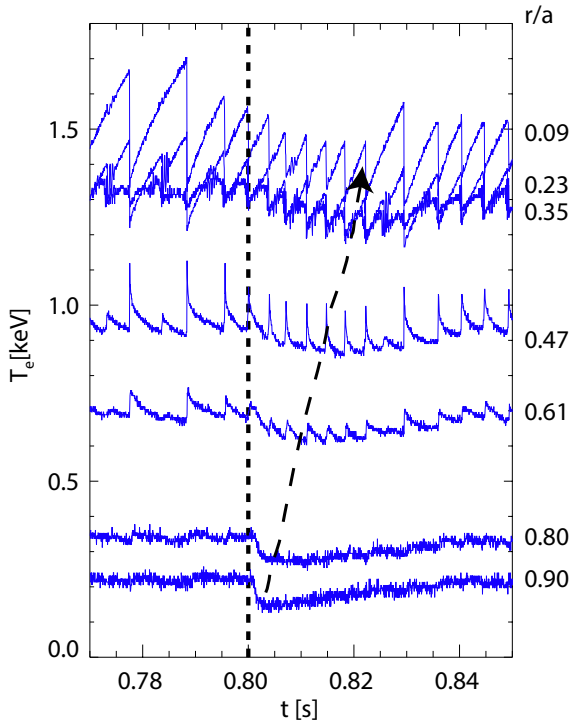

SOC: $\bar{n}_{e,20} = 1.3$

Ion Temperature and Rotation

- Ion temperature response is similar to T_e with slower time scale.
- Plasma rotates in co-current direction in LOC; counter-current direction in SOC.

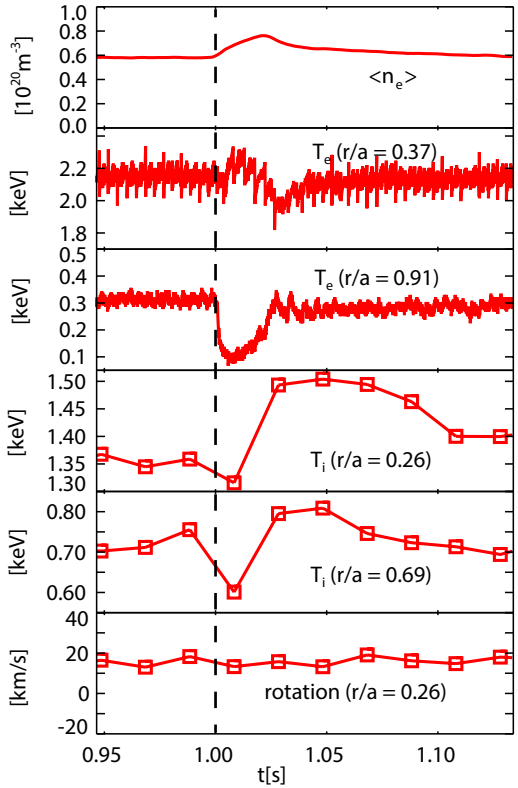

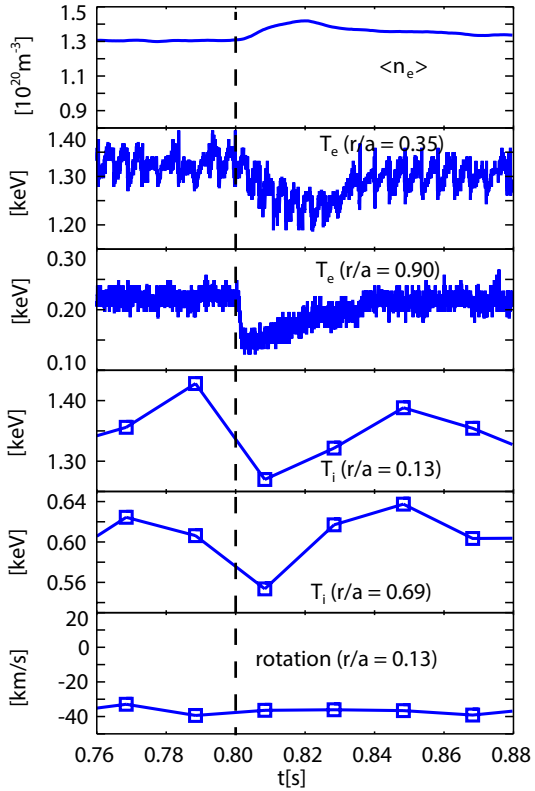

LOC: $\bar{n}_{e,20} = 0.6$

SOC: $\bar{n}_{e,20} = 1.3$

Non-local is Correlated with Rotation Reversal

- Density ramp-up experiments demonstrate that the non-locality is correlated with rotation reversal.

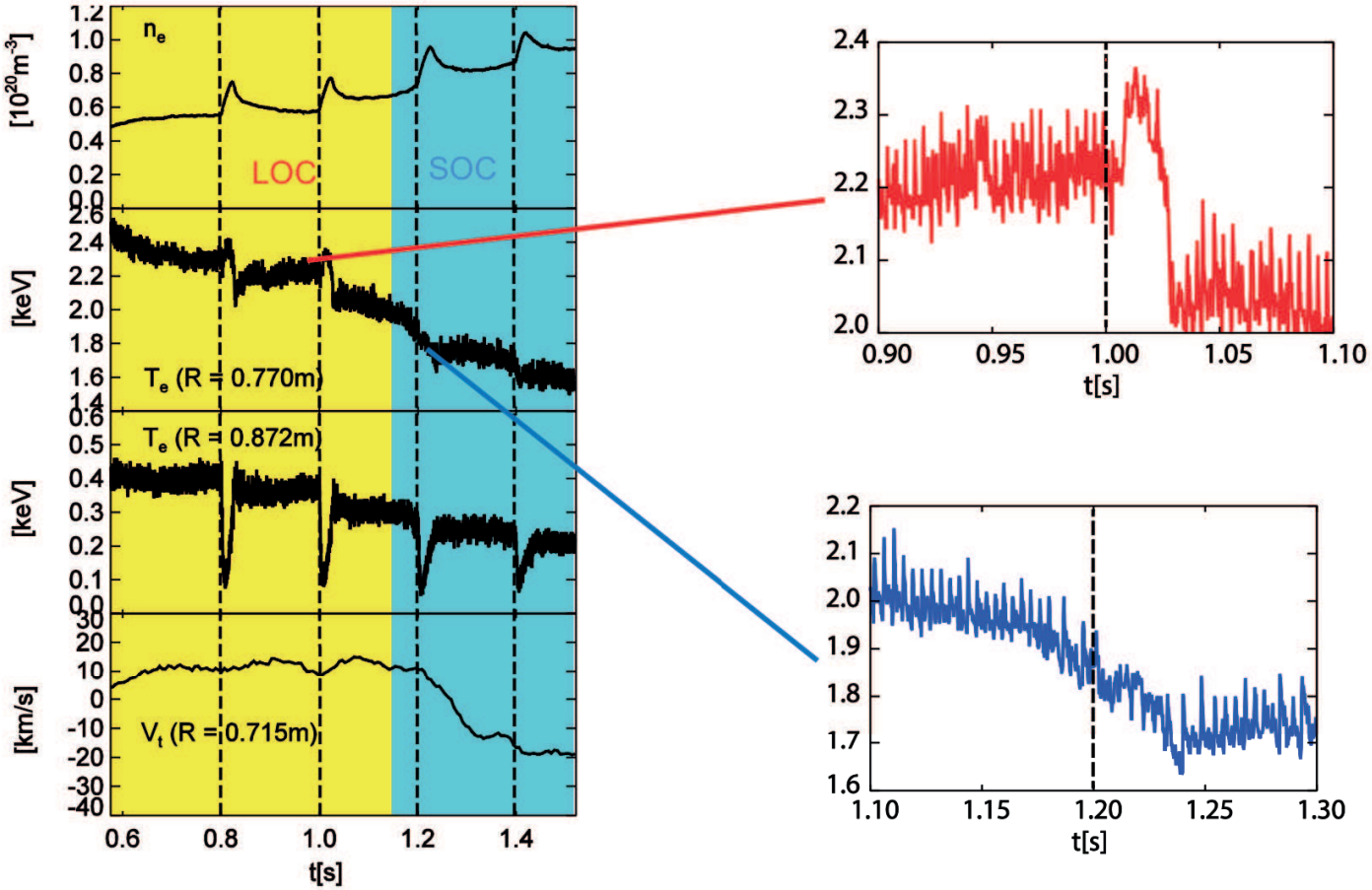

Correlation of Energy Confinement, Non-local Effect Polarity and Rotation Direction

- LOC-SOC, nonlocal-local and rotation transitions are correlated via density/collisionality.

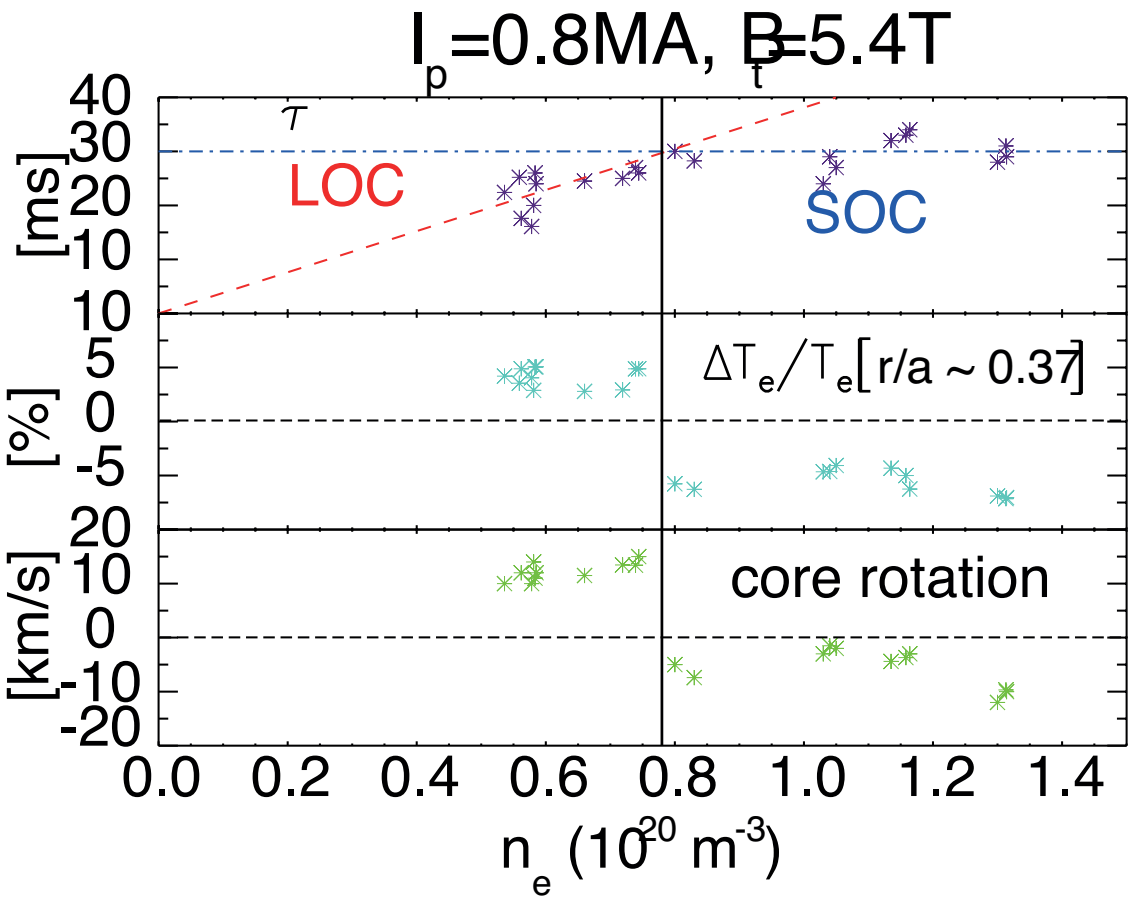

Transport Modeling of Non-Local Effect

- For LOC plasmas, the prompt increase of central electron temperature indicates a sudden and global reduction of core heat transport.
- Simulation result agrees well with measured data.

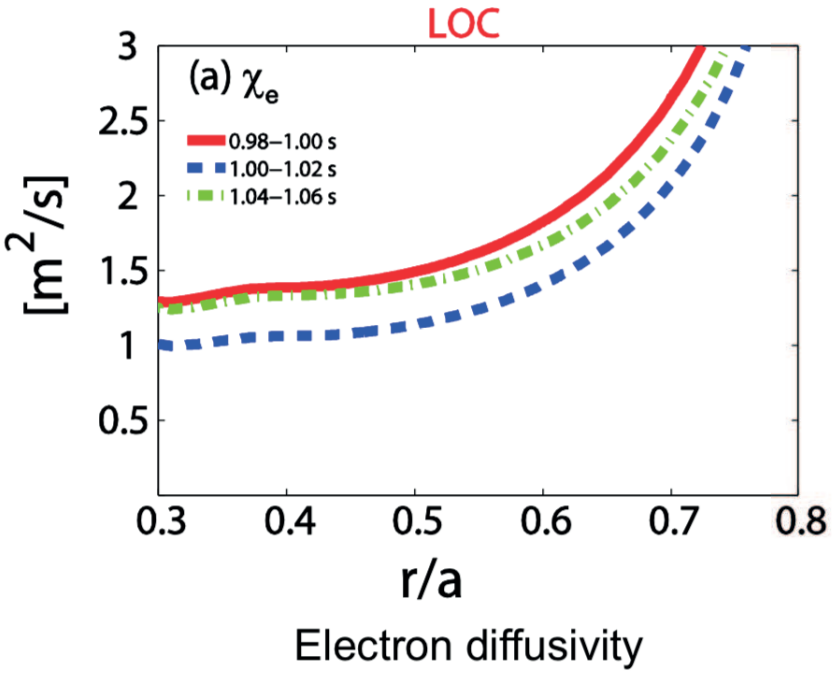

Electron diffusivity

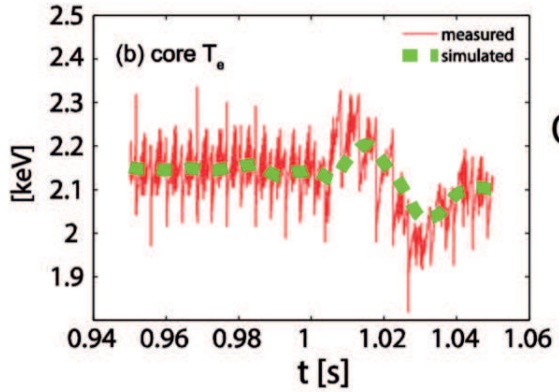

Core temperature

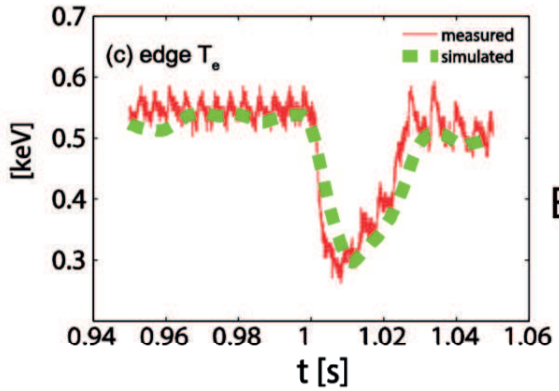

Edge temperature

Core Density Fluctuations Suppression during Cold Pulse

- For LOC plasmas, density fluctuations are found to be suppressed by cold pulse injections.

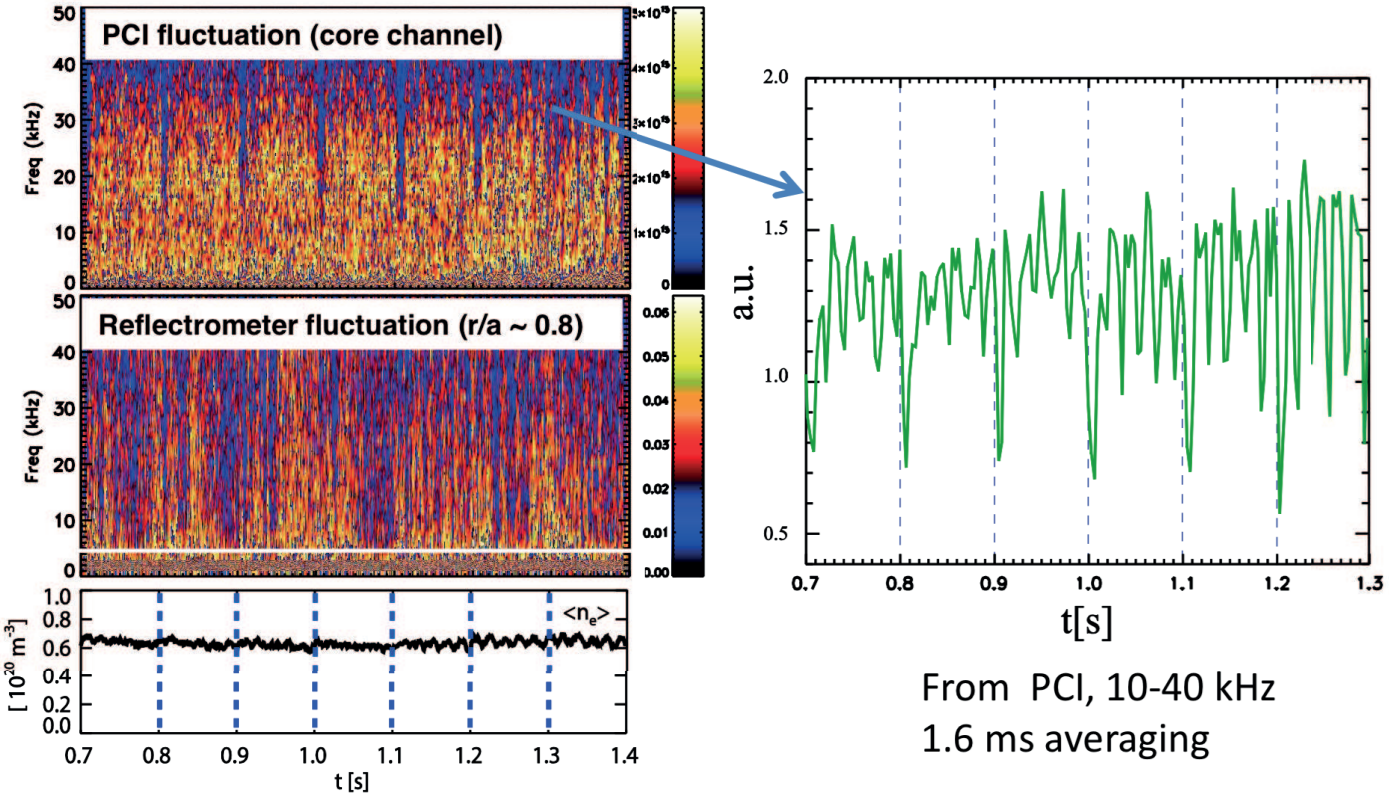

Heat Propagation of Sawtooth Crash Shows Confinement Improvement after Cold Pulse Injection in LOC Plasmas

- Time-to-peak from soft X-rays before and after cold pulse injection shows similar reduction in heat transport.

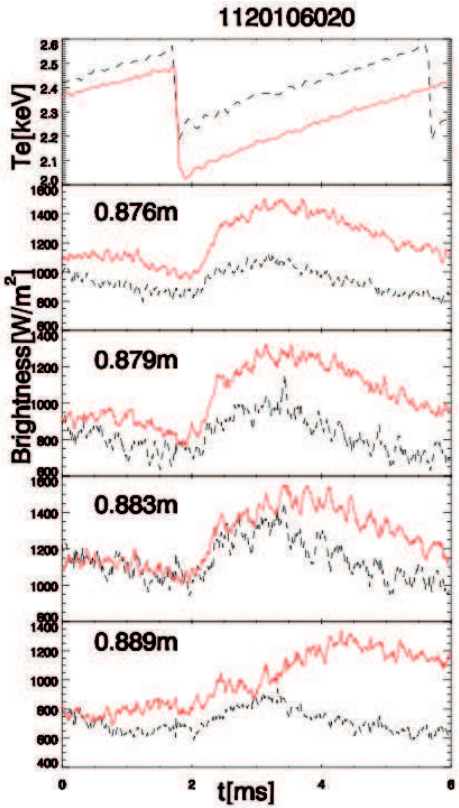

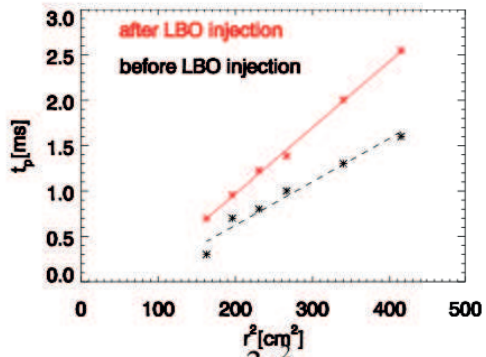

$$\chi_{ep} \sim \frac{3r^2}{8t_p}$$

t_p: time-to-peak

Before: $\chi_{ep} \sim 7.83\ \mathrm{m^2 s^{-1}}$

After : $\chi_{ep} \sim 5.13\ \mathrm{m^2 s^{-1}}$

Diffusivity is reduced by ~ 30% after cold pulse injection
Consistent with the reduction of local electron heat transport

*Callen J D and Jahns G L 1976 *Phys. Rev. Lett.* **38** 491

Linear Gyrokinetic Simulation to Characterize the Turbulence

- TEM to ITG transition as a unifying assumption for energy confinement saturation, rotation reversal and disappearance of non-locality
- At r/a = 0.5, both LOC and SOC plasmas are ITG mode dominant
- At r/a = 0.75, LOC is TEM dominant, SOC is ITG mode dominant

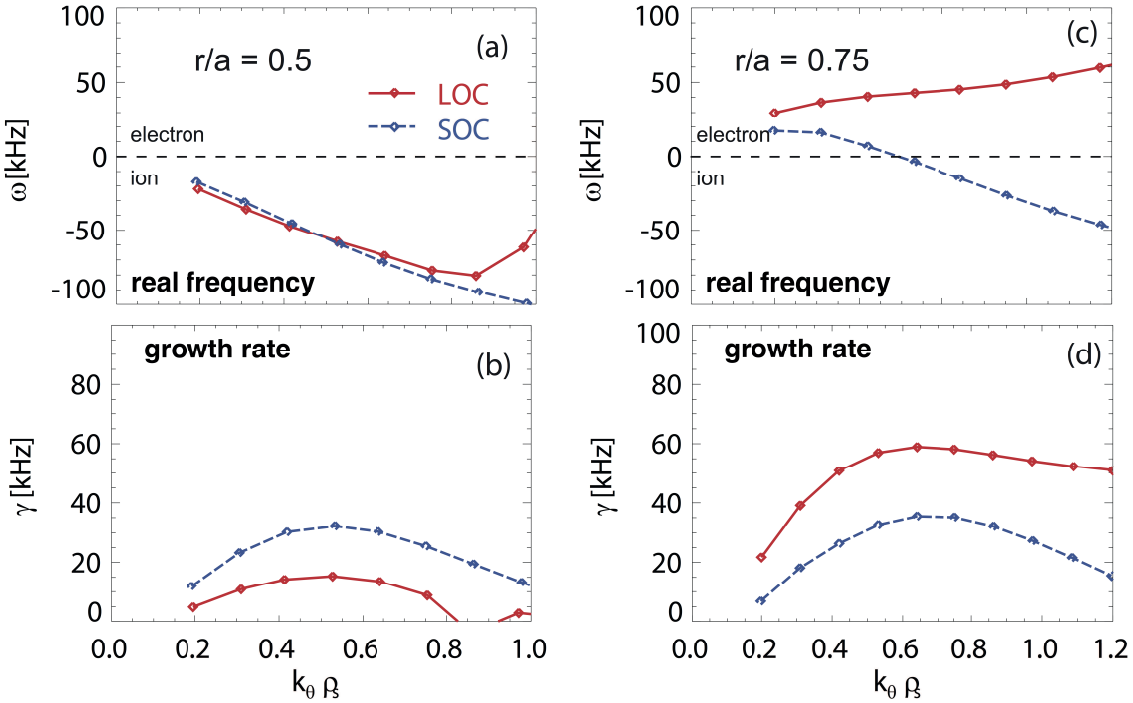

Growth Rate of Most Unstable Mode in LOC and SOC

- The sensitivity scan at r/a = 0.75 shows that LOC plasma is TEM dominant and SOC plasma is ITG mode dominant.

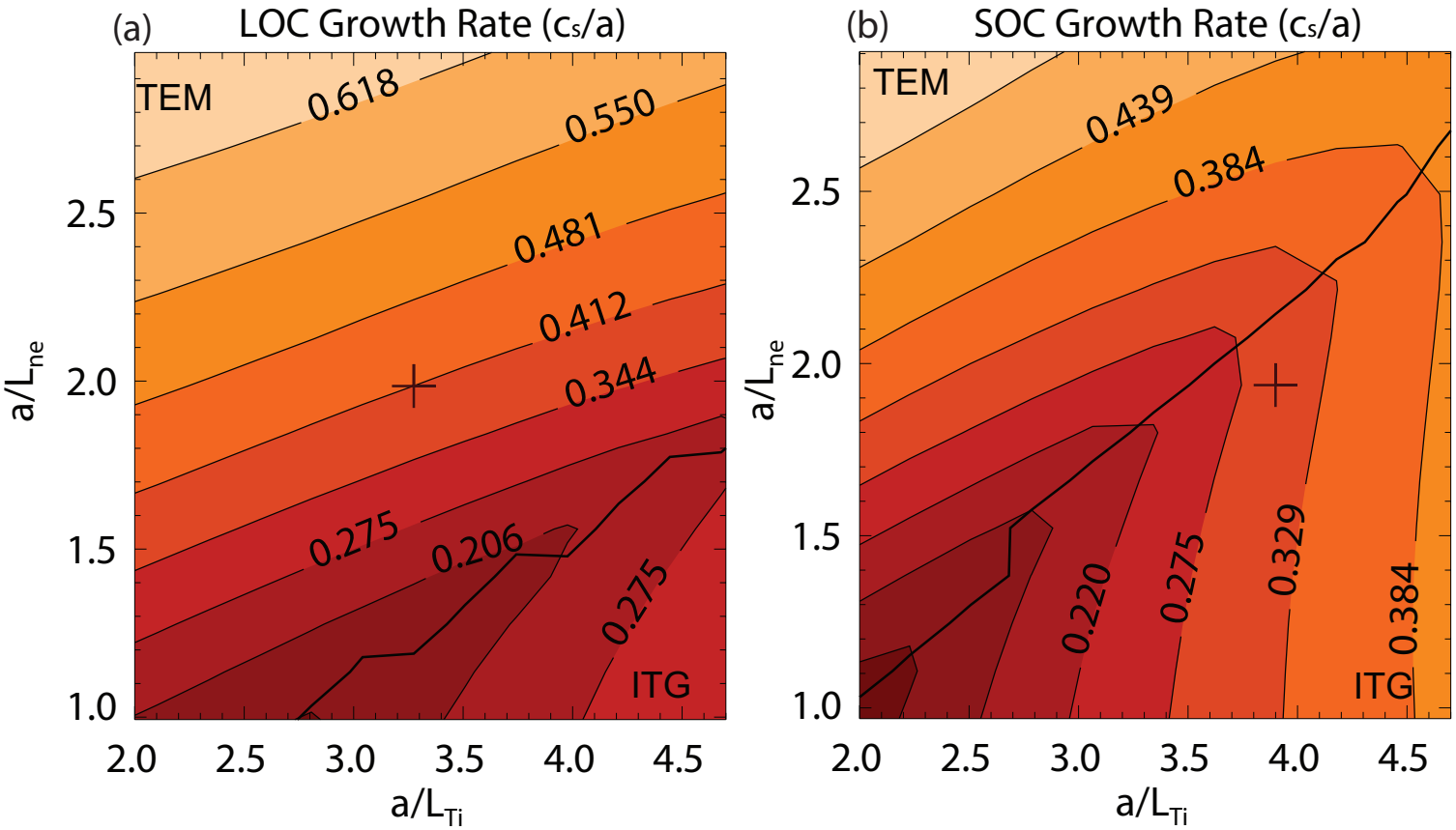

Summary of Non-local Heat Transport

- Non-local heat transport is observed with a density threshold.
- The density threshold is similar to LOC-SOC transient density and rotation reversal density, which indicates non-local effect is correlated with energy confinement and momentum transport.
- Transport analysis and fluctuation measurements show a reduction of core heat transport during cold pulse.
- Linear GYRO simulations suggest that at r/a=0.75, TEM is dominant in LOC plasmas, while ITG mode is dominant in SOC plasmas. Sensitivity scan shows the dominance change.

Overview

Future Work with X-ray Spectroscopy in Alcator C-Mod

1. Test wavelength calibration with cadmium anode x-ray tube.

He-like argon w	3.9492 Å	3.1395 keV
H-like cadmium Lα1	3.9564 Å	3.13373 keV

2. ITER-relevant neon-like xenon spectra.
   - 2p–3d transition, 2.73 Å (4.5415 keV)
   - $T_e \sim 4 - 10$ keV. Line peaks at 7 keV
3. ITER-relevant krypton spectra.
   - Krypton Kα lines: 0.98 Å (12.6 keV)
   - Broad Te profile with $T_{e0} > 6$ keV.
4. New experiment on argon pumpout.
   - Use PCI to detect mode conversion strength and location.
   - Study the possible edge effects.
5. The effect of current profile on impurity and momentum transport.
   - Calcium injection during LHCD.
   - Whether q or $\hat{s}$ determines the direction of core rotation in LHCD.

Thanks

Overview

Intrashot locked mode calibration toolkit

The intrashot calibration widget (C. Gao) is used to do quick locked mode calibration between shots.

Raytracing widget to estimate photon attenuation

The raytracing widget (C. Gao) is used to estimate:

- vignetting from spool between beryllium window & B-port flange.
- attenuation from beryllium window
- blocked view from obstacles (like RFQ tube)

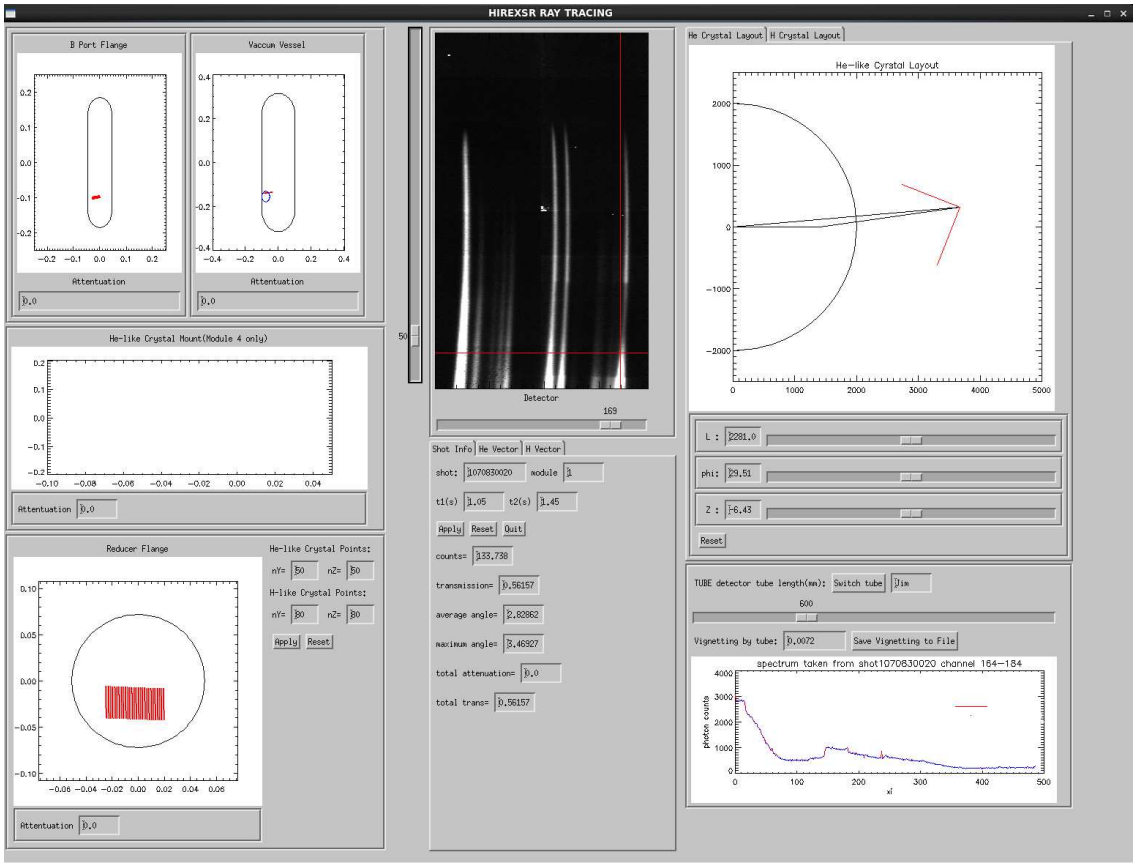

STRAHL: 1-D Time-Evolving Impurity Transport Code

The STRAHL analysis GUI is developed (C. Gao) to study the argon impurity transport and compare with HiReX–Sr measurements.

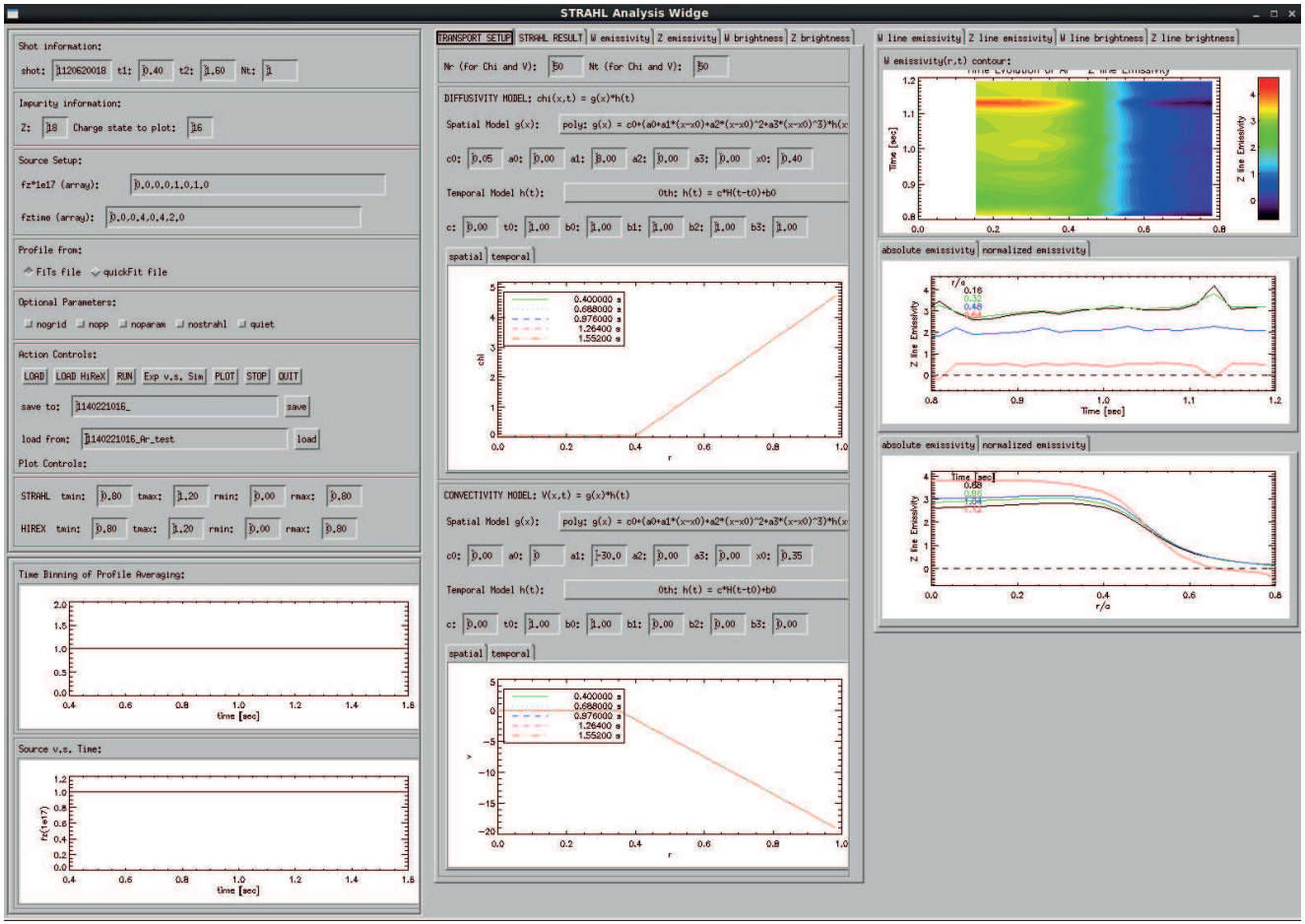

Possible Mechanisms

- Impurity - wave interaction.
- Modification of source/recycling (edge effect).
- Change of other plasma parameters: T_e, n_e, etc.

Possible Mechanisms

- Impurity - wave interaction.
- Modification of source/recycling (edge effect).
- Change of other plasma parameters: T_e, n_e, etc.

2^{nd} Harmonic Resonance with Finite $k_x \approx \frac{\pi}{\rho_L}$

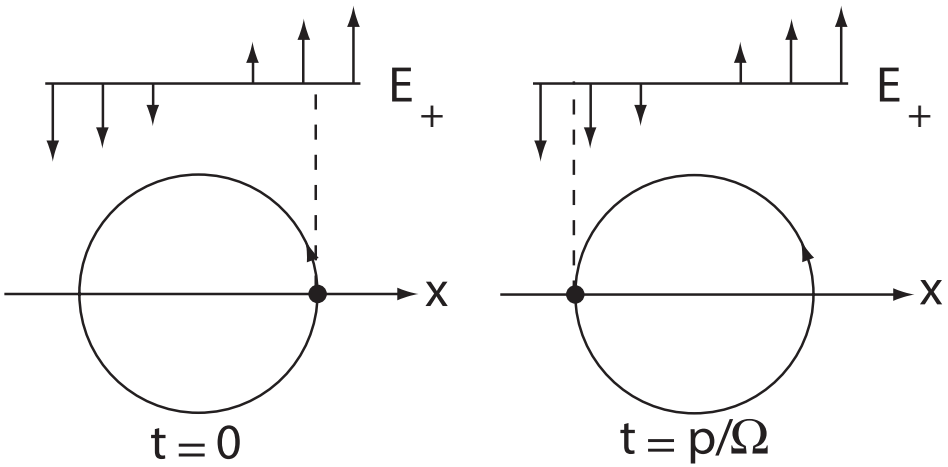

Figure from J. P. Freidberg. Plasma physics and fusion energy.

1. Ar^{16+} 2^{nd} harmonic resonance layer overlaps with the H–D mode conversion layer when $\frac{n_H}{n_D} \approx 46\%$.
2. Enhanced E_r at H–D mode conversion layer.
3. When $\Omega_{RF} = 2\Omega_I$, $k_x \approx \frac{\pi}{\rho_L} \neq 0$, argon can be perpendicularly accelerated and deconfined $(\mathbf{v}_\perp \cdot \mathbf{E})$.

Optimum H/D ratio $\frac{n_H}{n_D} = 46\%$ for Ar^{16+}

The mode conversion layer $\left(n_{\parallel}^2 = S\right)$ for H+D plasma is located at:

$$n_{\parallel}^2 = 1 - \frac{\omega_{pH}^2}{\omega_{RF}^2 - \omega_H^2} - \frac{\omega_{pD}^2}{\omega_{RF}^2 - \omega_D^2} \tag{1}$$

The MC layer (R_{MC}) and impurity resonant layer ($R_{resonant}$):

$$\gamma \equiv \frac{n_H}{n_D} \qquad R_{MC} = \frac{eB_0}{m_p \omega_{RF}} \sqrt{\frac{1 + \frac{1}{2}\gamma}{1 + 2\gamma}} R_0 \qquad R_{resonant} = n\frac{Z}{A}\frac{eB_0}{m_p \omega_{RF}} R_0 \tag{2}$$

$R_{MC} = R_{resonant}$ requires:

$$\gamma\left(A^{Z+}\right) = \frac{1 - \left(n\frac{Z}{A}\right)^2}{2\left(n\frac{Z}{A}\right)^2 - \frac{1}{2}} \tag{3}$$

$$\gamma\left(Ar^{16+}\right) = 46\%$$

$$\gamma\left(Ar^{17+}\right) = 29\%$$

B-dependence of Resonance Position

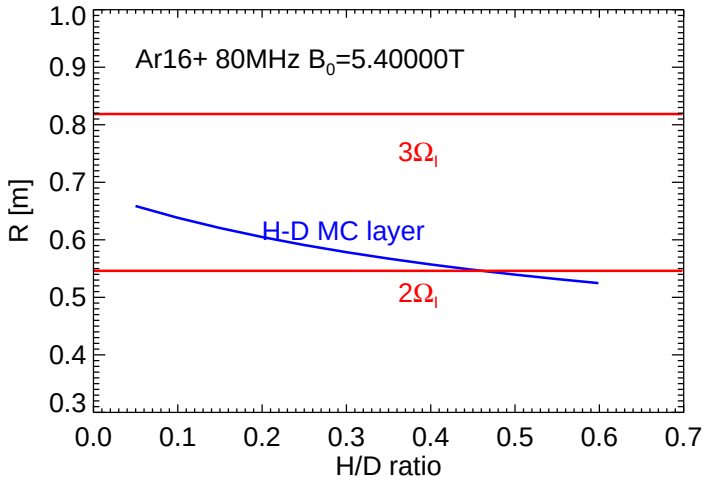

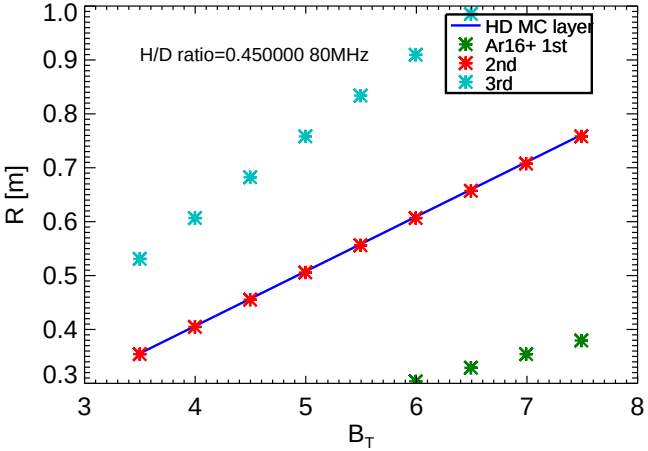

- Required $\frac{n_H}{n_D}$ doesn't depend on B.
- B moves the resonance position.

B-dependence of Resonance Position

The resonance/mode-conversion layer locates in HFS.

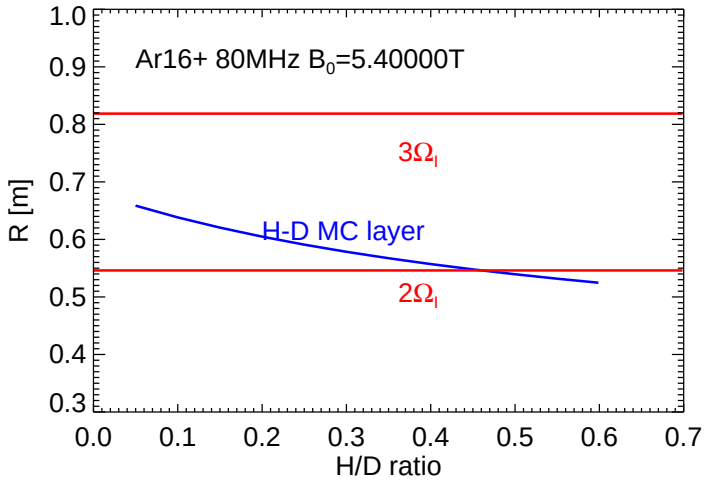

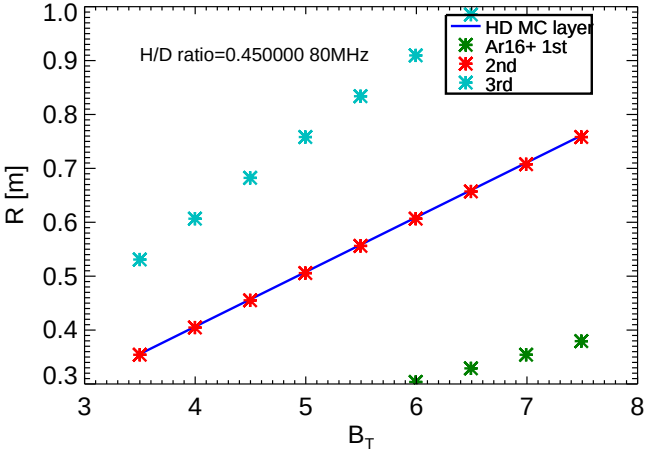

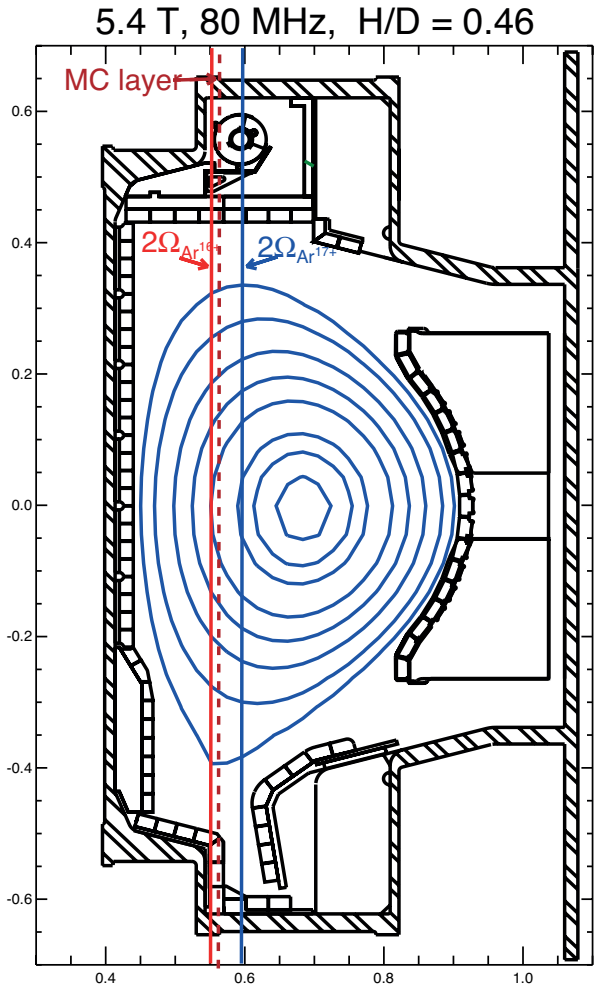

Deconfinement Energy for Argon

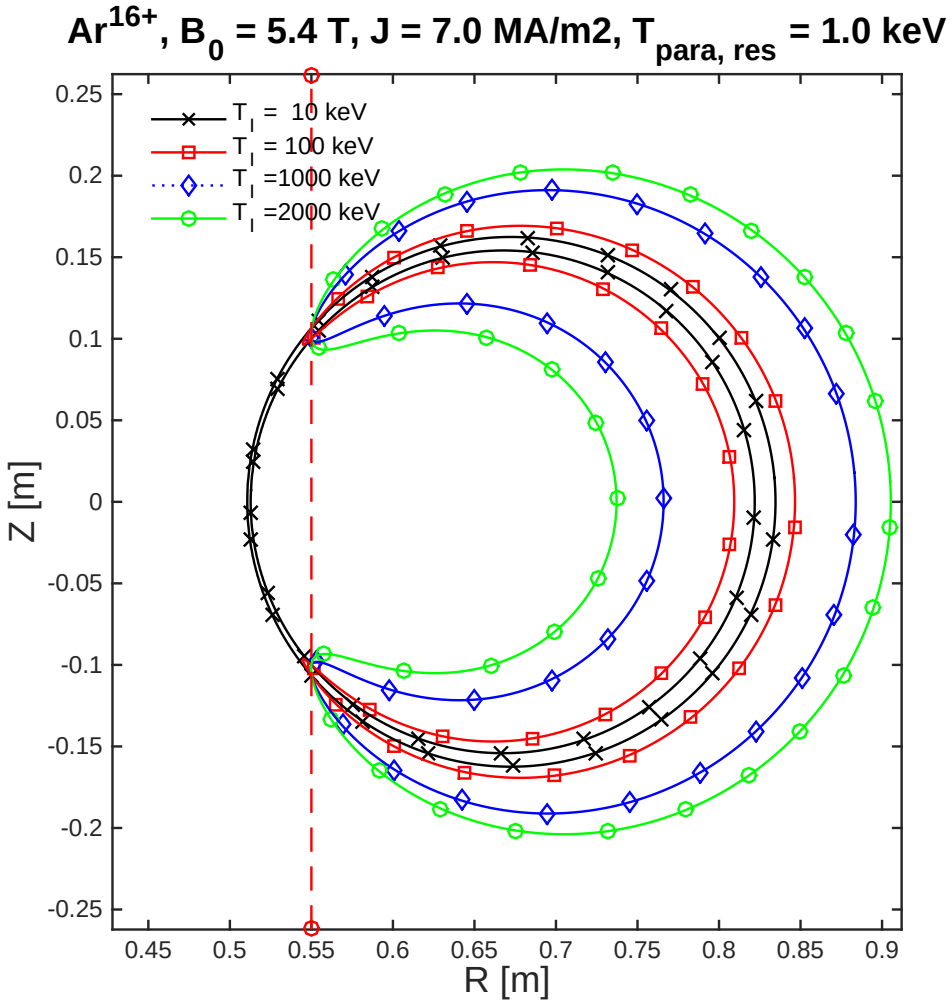

Possible Mechanisms

- Impurity - wave interaction.
- Modification of source/recycling (edge effect).
- Change of other plasma parameters: T_e, n_e, etc.

Modification of source/recycling

- At high H/D ratio, the single path absorption of ICRF wave, launched from low field side, will be poor.
- Plasma edge potential may change the impurity influx [L. Oren, 1982].
  - Impurity accumulations under negative edge potential ($-200 - -800V$)
  - Steady state (recycling) under zero or positive edge potential.
  - But no pumpout...
- Wall recycling modified by ICRF?

1. Simulation with An Outward Convection

STRAHL simulation qualitatively reproduced the evolution of Ar^{16+} brightness [a.u.] with Gaussian shape convection.

STRAHL

$D=1\ m/s^2$, $V_{t<1.0}=0\ m/s$, $V_{t\geq 1.0} = 15e^{-\frac{(r/a-0.4)^2}{2\times 0.25^2}}\ m/s$

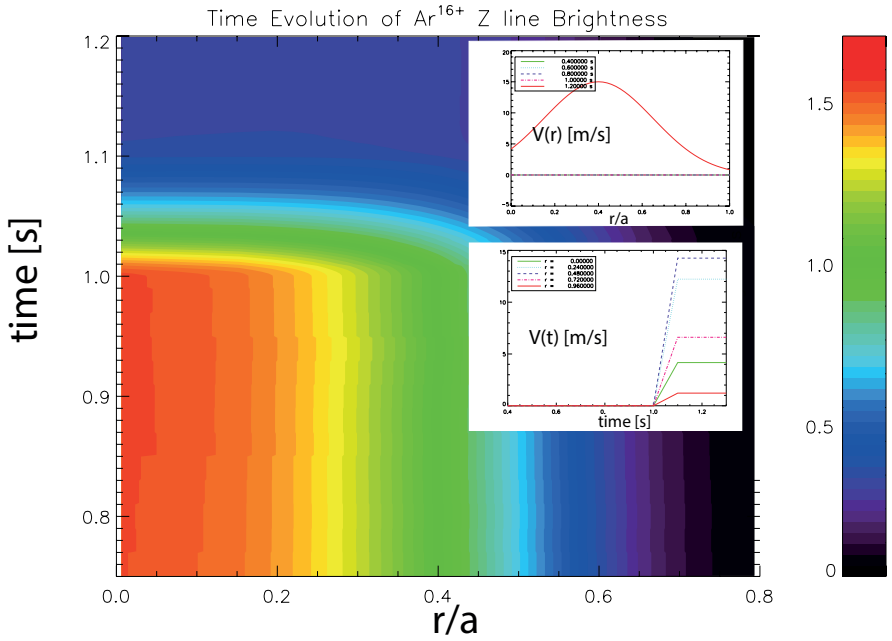

Experiment (HiReX–SR)

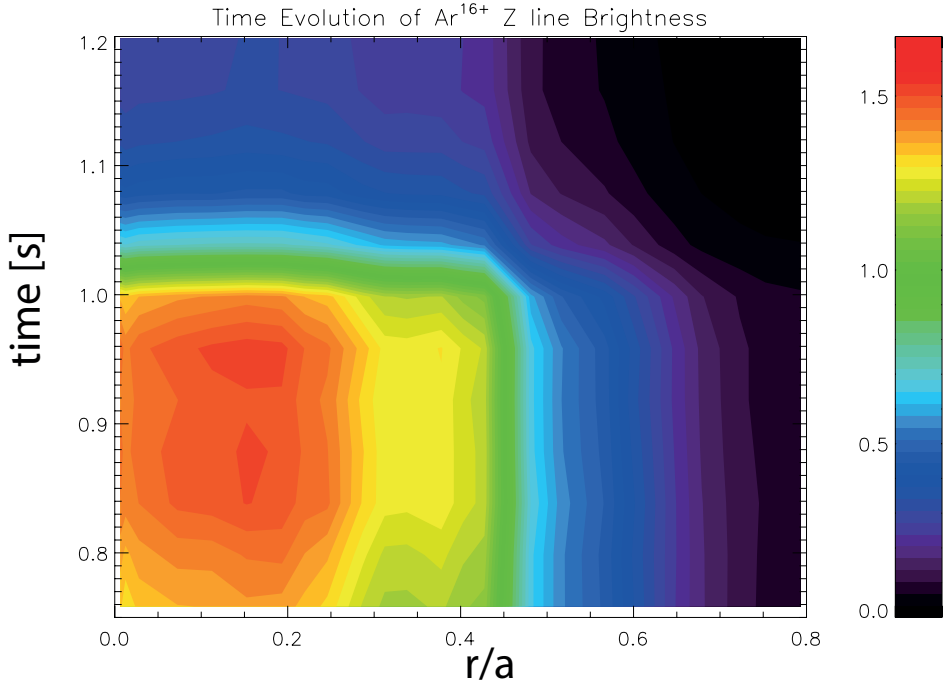

1. Simulation with An Outward Convection

But the evolutions of normalized brightness show disagreement between STRAHL simulation and experiment.

STRAHL(normalized)

D=1 m/s^2, $V_{t<1.0}$=0 m/s, $V_{t\geq 1.0} = 15e^{-\frac{(r/a-0.4)^2}{2\times 0.25^2}}$ m/s

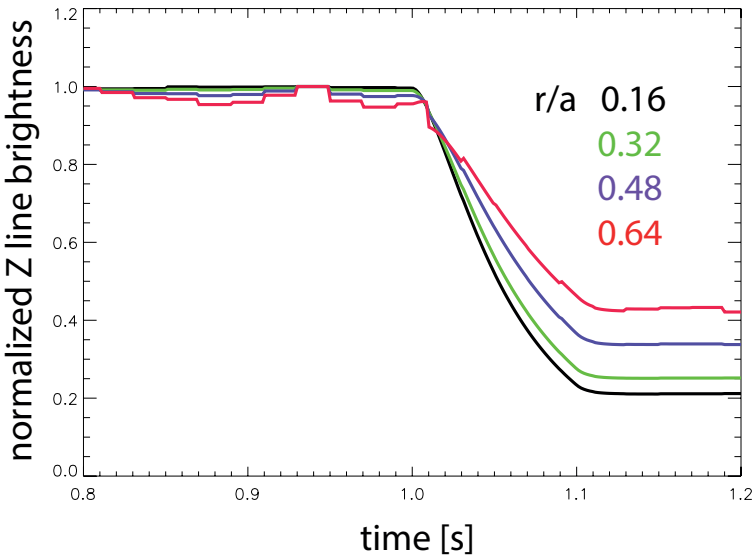

Experiment(normalized)
(HiReX–SR)

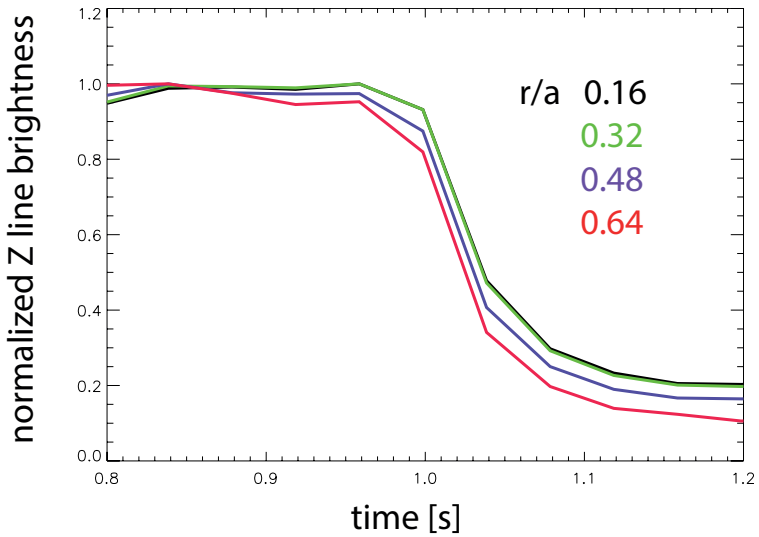

1. Simulation with An Outward Convection

Also the evolutions of Ar^{14+} and Ar^{15+} density underestimate the pumpout effect.

STRAHL: Ar^{15+} density

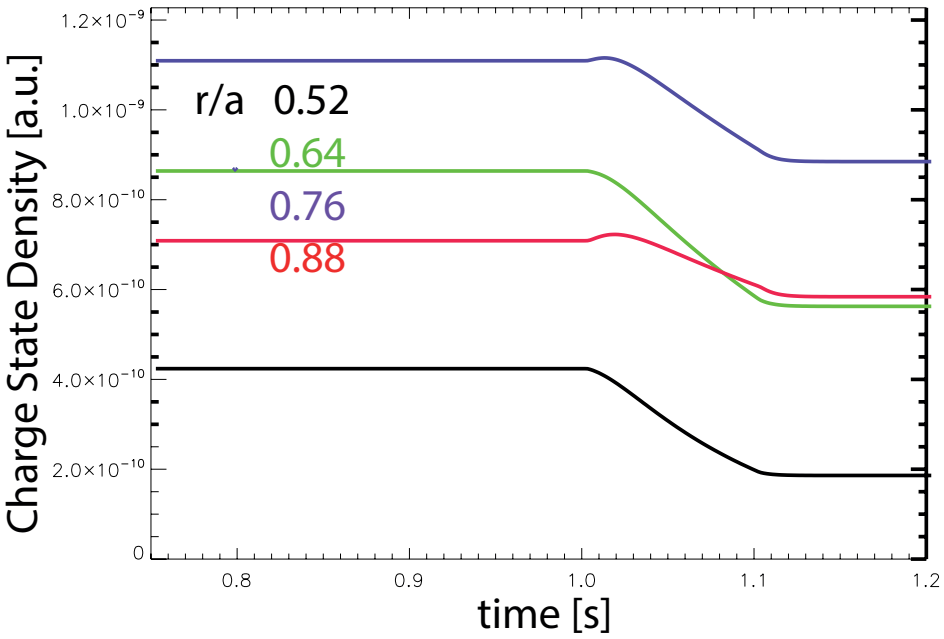

STRAHL: Ar^{14+} density

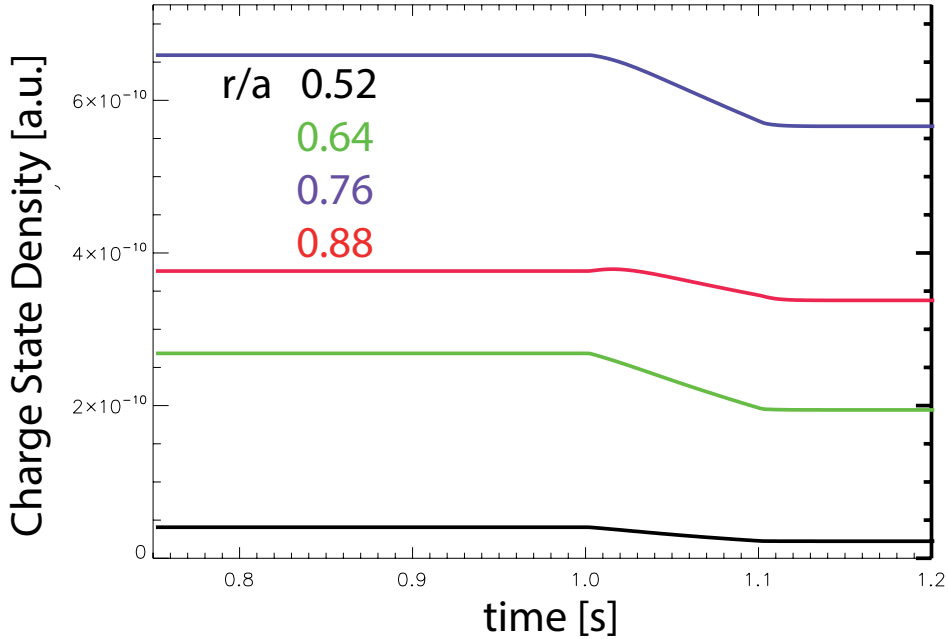

2. Simulation with Source Reduction

The evolutions of Ar^{14+} and Ar^{15+} density with a source reduction agree with the observation.

STRAHL: Ar^{15+} density

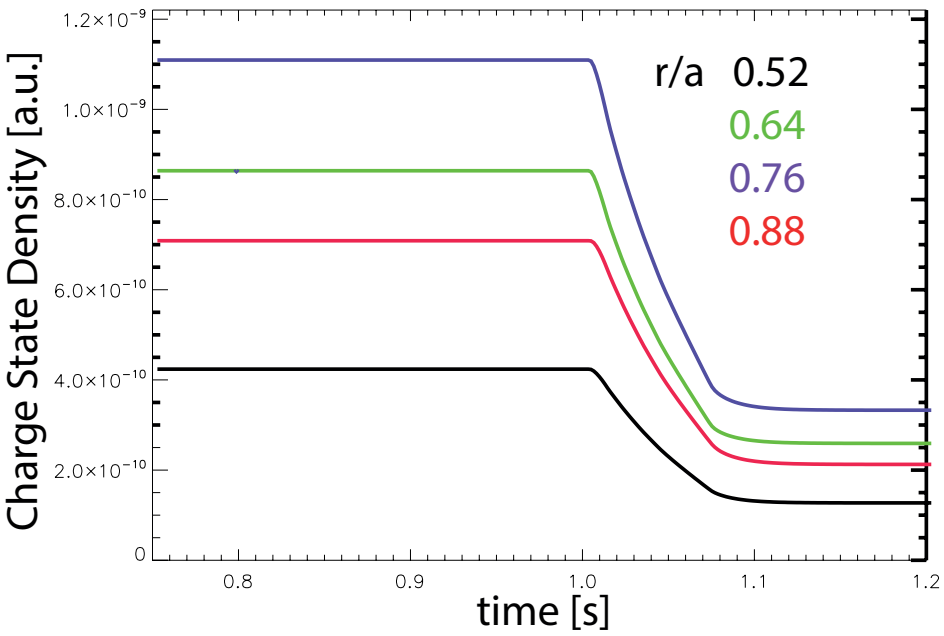

STRAHL: Ar^{14+} density